University of Pretoria

CHARACTERIZATION OF JAROSITE FORMED DURING BIOOXIDATION OF REFRACTORY GOLD ORES AND ITS EFFECT ON CYANIDE CONSUMPTION DURING GOLD LEACHING

BY

MICHAEL KANDENGWA

SUPERVISED BY

PROFESSOR RF SANDENBERGH

A dissertation submitted in partial fulfilment of the requirements for the degree of

Master of Applied Sciences (Metallurgy)

in the

Department of Materials Science and Metallurgical Engineering

Faculty of Engineering, Built Environment and Information Technology

University of Pretoria

Republic of South Africa

2016

ABSTRACT

Biooxidation is an attractive process for unlocking of gold from refractory ores, but could be further improved by reducing the rather high cyanide consumption during the cyanidation of the biooxidation residues. The high cyanide demand is typically ascribed to the presence of metastable intermediate sulfur species formed during the oxidation of the sulfide, but it is also conceivable that jarosite formation during the acidic biooxidation process and subsequent leaching during the alkaline cyanidation could also account for significant cyanide consumption. The present work was done to establish if jarosite would readily form under typical biooxidation conditions and, if so, if it would then leach during cyanidation. Methods to stabilise or remove the jarosite were also investigated. To this end crystalline potassium jarosite was synthesized simulating conditions for the mesophile BIOX® process and its decomposition in alkaline media at pH 10.5 to 11 at 25ºC investigated. It was found that it transformed into another amorphous iron compound as indicated by a change in colour from yellow to reddish, the presence of potassium and sulfate ions in solution, as well as the disappearance of the characteristic XRD pattern of jarosite. The jarosite also leached in aqueous alkaline cyanide as indicated by the presence of iron in solution, with increased leaching at higher cyanide concentrations. The jarosite could not be totally passified by aging, but removing it by leaching with an iron-complexing agent like oxalic acid was found to be possible. The consumption of cyanide by jarosite during gold leaching could thus be significant, but would obviously depend on how much jarosite is formed during the bioleaching process.

Jarosite was observed to be present in the mesophile and thermophile BIOX® products from Fairview Mine with more jarosite present in the products of the thermophile process. The process jarosite was significantly more stable than that produced in the laboratory during alkaline cyanidation with 17 mass percent of the jarosite converted to ferric hydroxide for the process jarosite compared to complete conversion for the laboratory jarosite for a 24 hours leaching period. However, it still accounted for a significant amount of the cyanide consumed.

Keywords

Jarosite, biooxidation, cyanide, gold leaching.

ACKNOWLEDGEMENTS

Firstly I would like to thank the Almighty Lord for abilities and strength he gave me and the opportunity to develop them.

I would like to express my sincere appreciation to Professor RF Sandenbergh for his invaluable advice, guidance, expertise, and constructive criticism throughout the course of this research.

I acknowledge with thanks the financial support of Biomin, the Department of Material Sciences and Metallurgical Engineering (University of Pretoria) and the Department of Trade and Industries through the THRIP programme. The support of Barberton Mines with the provision of samples and data is gratefully acknowledged.

My friends, colleagues and personnel in the Department of Materials Sciences and Metallurgical Engineering are equally appreciated for their continuous support and encouragement throughout my studies.

I would like to thank my family, in particular my wife Sharon, my brother Marko and my children for their continual love, tolerance, endurance and patience throughout my studies.

TABLE OF CONTENTS

LIST OF FIGURES

LIST OF TABLES

APPENDICES

1 INTRODUCTION

1.1 General Background

Jarosites are hydroxysulfate precipitates of the alunite group found to be useful in some mineral processing operations but a major problem in others. In zinc production the precipitation of iron as jarosites enabled the increased recovery of zinc from zinc ferrites as the iron leached could be precipitated at relatively low pH values in filterable and washable form. In the biooxidation of refractory gold ores jarosites may be formed during the elevated temperature acidic sulfate leach, and subsequently carried with the other solids to the cyanidation process and possibly leached with the gold in the alkaline cyanide lixiviant (Miller and Brown, 2005).

Jarosites with the general formula $MFe_3(SO_4)_2(OH)_6$, with M a monovalent or divalent ion, or their combinations, typically precipitate in ferric-rich acidic sulfate solutions at elevated temperatures in the presence of an appropriate salt, via reaction[1]:

$$3Fe^{3+} + M^{+} + 2SO_4^{2-} + 6H_2O = MFe_3(SO_4)_2(OH)_6 + 6H^{+} \quad [1]$$

The properties and phases of these precipitates are dependent on the ionic composition and concentrations (ferric iron, sulfate, and alkali cations), pH, temperature, contact time and the general solution chemistry (Dutrizac, 1983a,b; Gramp, et al., 2008; Wang, et al., 2007). The acidic conditions, high sulfate and ferric ion concentrations, and the monovalent cations from the mineral salts used to provide nutrient ions for bacteria, or solubilisation of accessory minerals make the operating conditions used in the mesophile and thermophile biooxidation processes favourable for the formation of jarosite (Niemela, et al., 1994; Bigham, et al., 2001).

Biooxidation residues typically contain jarosites, residual labile sulfur intermediate products due to the incomplete oxidation of sulfide to sulfate (elemental sulfur, polysulfides and thiosulfate), base metals, and some residual metal sulfide minerals depending on the ore composition and extent of sulfide oxidation achieved (Jones and Hackl, 1999). The recovery of gold subsequent to the biooxidation pretreatment typically requires relatively high cyanide additions for effective leaching of the gold due to the presence of high levels of cyanicides carried over to cyanidation in the residual solids with thiocyanate and iron cyanide complexes typically being indicated to be the main reaction products. The labile sulfur species which form during sulfide oxidation to

sulfate according to the proposed mechanisms have been reported to react with cyanide to form mostly thiocyanate (SCN^-) (Sand, et al., 2001). Base metal sulfides would typically be leached during biooxidation but some, typically mostly iron, could be transferred with the solids as adsorbed species or in the form of precipitates such as jarosites. These species are typically not stable under alkaline cyanide leaching conditions and may thus significantly contribute to cyanide consumption by forming iron cyanide complexes (Ciftci and Akcil, 2010).

Jarosite is indeed only stable over a relatively narrow acidic pH range and readily breaks down when exposed to lower or higher pH conditions as illustrated in Figure 1.1. The decomposition mechanism and rate of the jarosite is dependent on the solution conditions with pH playing a major role.

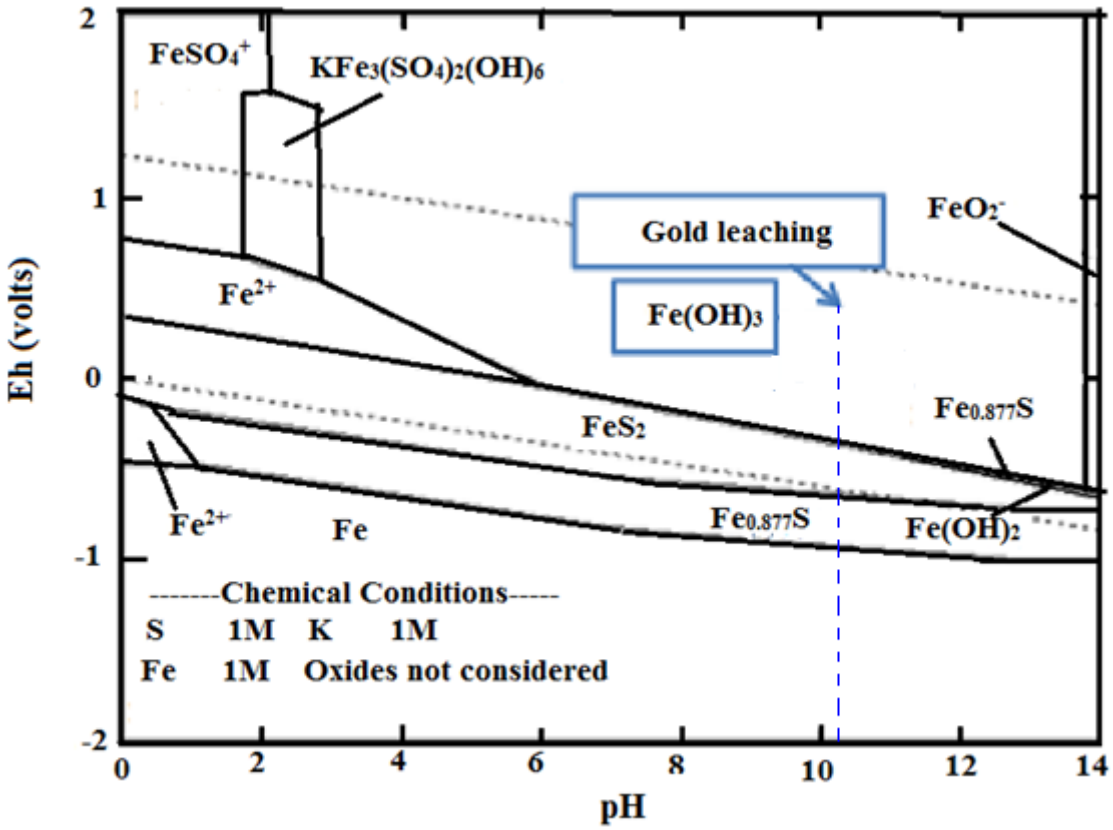

Figure 1.1. Pourbaix diagram for the Fe (1M), S (1M), and K (1M) system (NBS data at 25°C, software: Stabcal W32, Gibbs free energy data in Appendix 1)

Leaching of gold in aqueous cyanide is typically done under alkaline conditions for safety reasons and would thus favour the conversion of jarosite to labile iron species (amorphous ferric hydroxide). The amorphous ferric hydroxide is reactive and reacts with cyanide to form the ferric cyanide complex which is thermodynamically stable

under these conditions. The stability of iron cyanide complexes in dilute aqueous cyanide solution is shown in Figure1.2. Cyanide also forms anionic metal cyanide complexes mainly with transition metals whose stabilities vary and which require moderate to highly acidic conditions to dissociate (Sehmel, 1989). The iron cyanide complexes may also act as ligands to form insoluble metal-iron cyanide precipitates with Fe, Cu, Ni, Mn, Pb, Zn, Cd, Sn, and Ag over a pH range of 2 to 11, for example $Fe_4(Fe(CN)_6)_3$, i.e. Prussian blue. The formation of these secondary precipitates may hinder the dissolution of gold (Kuyucak and Akcil, 2013; Wang and Forssberg, 1990).

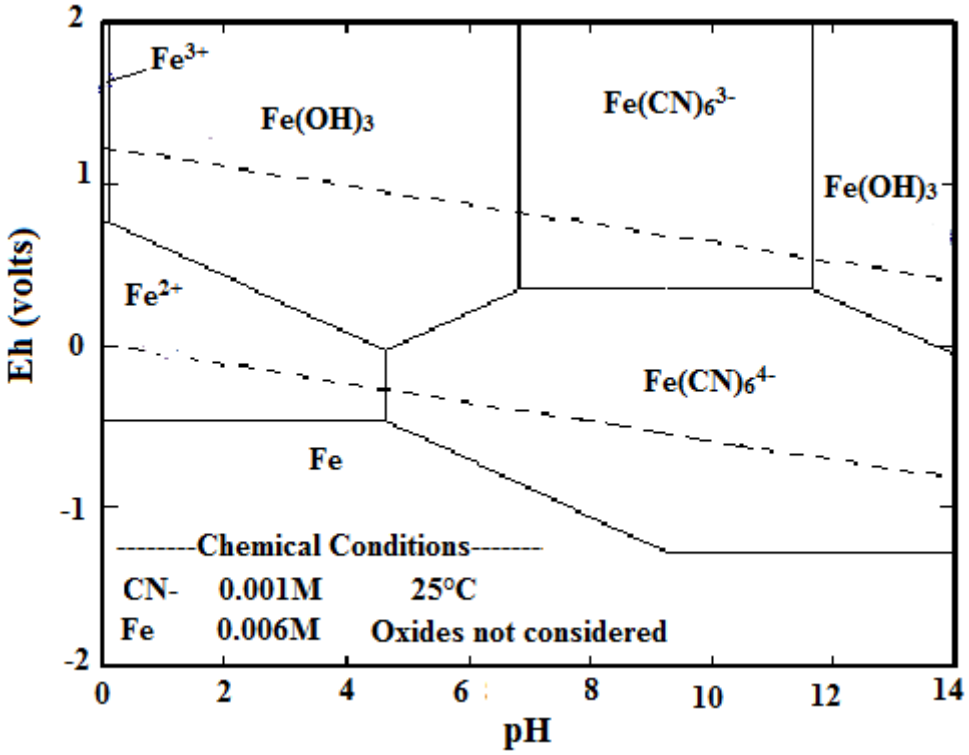

Figure 1.2. Pourbaix diagram for the Fe (0.006M) and CN^- (0.001M) system (NBS data at 25°C, software: Stabcal W32, Gibbs free energy data in Appendix 2)

1.2 Objectives of this study

The aim of this work is to investigate the probability of jarosites forming under bioleaching conditions and whether these will then decompose and act as cyanicides under alkaline cyanide leaching conditions. To this end both synthetic and process jarosites were evaluated. The synthetic jarosite was synthesized using chemistry similar to that used in the mesophile BIOX® process, while the process jarosites were produced using sulfide ore pulp and mesophile and thermophile bacteria. The different jarosites were then characterised and evaluated in terms of stability and their contribution to the consumption of cyanide during gold leaching. Measures to remove the jarosite by complexing the iron with carboxylic acids and also to stabilise the jarosite decomposition products by preconditioning in alkaline aqueous solution were assessed.

2 LITERATURE REVIEW

2.1 General background

Gold (Au) is a precious metal that naturally exists in different physical and mineralogical forms, typically in its elemental state, alloyed (with silver, tellurium, selenium, bismuth, mercury, copper, iron, rhodium, and platinum), but occasionally also associated with sulfides, carbonaceous matter and many other minerals (Marsden and House, 2009). Gold bearing ores are generally classified according to their mineralogy and/or processing routes as: free-milling gold (e.g. placers, quartz vein gold ore, oxidized ore, silver rich ore), and refractory gold ores, physically locked within sulfides (principally pyrite and arsenopyrite), chemically locked as gold alloys or compounds e.g. electrum, gold tellurides, aurostibnite, and maldonite, substitution in the sulfide lattice (solid solution) (La Brooy, et al., 1994).

Recovery of some of the gold present in free-milling placer ores may be achieved by gravity separation without pretreatment, but more typically a discardable tail would not be achievable and comminution to liberate the gold, followed by some concentration process, followed by separate leaching and recovery of the gold from the streams in a more concentrated form would be applied. Refractory gold ores are characterised by low gold recoveries using conventional aqueous cyanidation with high cyanide and oxygen consumptions due to reactive oxides and sulfides or preg-robbing behaviour due to carbonaceous and clay materials. Refractory gold ores typically requires a pre-treatment step to liberate the gold, and to remove or deactivate competing species to achieve economically acceptable gold recoveries. Even so, significantly higher lixiviant concentrations of cyanide and/or oxygen are typically required to achieve acceptable gold recoveries (La Brooy et al., 1994).

In sulfidic refractory ores/concentrates the valuable mineral is typically either occluded or associated with the sulfide minerals with the sulfide matrix exhibiting low leachability in many lixiviants (Bosecker, 1997; Nicol et al., 2006). To accomplish an efficient leaching process when using this kind of mineral or concentrate, the sulfide matrix must be totally or partially removed in a pretreatment stage to liberate the valuable mineral and make it amenable to subsequent leaching processes. Typical pretreatment processes used to oxidise the sulfide include roasting, pressure oxidation, or bacterial oxidation (biooxidation) or a combination of these processes with the iron

sulfide minerals oxidised to create sulfur dioxide gas in roasting, sulfate ions or sulfate containing precipitates in pressure oxidation, and sulfate, but also some intermediate sulfide oxidation products, in biooxidation. The iron component is typically oxidised to the trivalent state and forms solid compounds such as haematite during roasting and basic iron sulfate or jarosite and/or soluble compounds such as ferric sulfate during pressure oxidation and biooxidation.

The biooxidation process to enhance gold recovery from sulfidic ores involves the bioorganisms assisted oxidation of the sulfides to sulfate with accompanying liberation of the gold from the sulfide host matrices increasing the overall recovery that can be realised in subsequent processes. Several naturally occurring bacteria such as mesophilic (Acidithiobacillus ferrooxidans, Acidithiobacillus thiooxidans and Leptospirillum ferrooxidans) that thrive in the temperature range 35ºC to 45ºC, thermophilic (Sulfobacillus acidophilus) that thrive in the temperature range (45ºC to 65ºC), and extreme thermophiles (sulfolobus) which thrive at higher temperatures (65ºC to 80ºC) are capable of catalysing sulfide mineral oxidation and are typically used for this purpose (van Aswegen and van Niekerk, 2004). The ferrous iron is converted to the ferric state by ferrooxidans bacteria and the sulfide-sulfur is ultimately converted to an acid sulfate solution by the thiooxidans bacteria (Amankwah et al., 2005). This technique has been applied successfully on a commercial basis for the removal of major sulfide minerals associated with refractory gold ores, such as arsenopyrite, pyrrhotite, and pyrite to give high gold extractions on cyanidation since 1986 (van Aswegen, et al., 1989). The bacterial oxidation reactions of sulfide minerals (pyrite, arsenopyrite and pyrrhotite) show high demand for oxygen, with the arsenopyrite and pyrrhotite consuming acid and the pyrite producing acid as shown in equations [2] to [4]. During the oxidation of sulfide minerals several chemical and bacterial assisted reactions take place producing precipitates (jarosites, scorodite, gypsum, and elemental sulfur) and other sulfur species.

$$4FeS_2 + 15O_2 + 2H_2O = 2Fe_2(SO_4)_3 + 2H_2SO_4 \quad [2]$$

$$2FeAsS + 7O_2 + H_2SO_4 + 2H_2O = 2H_3AsO_4 + Fe_2(SO_4)_3 \quad [3]$$

$$4FeS + 9O_2 + 2H_2SO_4 = 2Fe_2(SO_4)_3 + 2H_2O \quad [4]$$

The bacterial oxidation technology has been shown to require less capital, reduced operating costs, be more efficient, environmentally friendly and involving less skilled operating and maintenance personnel than conventional roasting and high pressure oxidation processes (Lynn, 1997).

2.2 Oxidation of sulfide minerals by bacteria

The degradation of sulfide minerals effected by bacteria occurs through a series of pathways with the electrons liberated during the oxidation transferred to a terminal electron acceptor via the electron transport system of the microorganisms. The bacteria may oxidise the sulfide minerals directly by enzymatic action with oxygen, that is, the sulfide is microbiologically converted to sulfate without detectable intermediates releasing the metal cations into solution. In this scenario close contact is required as the cells must physically attach to the mineral surface. On the other hand the sulfide oxidation may occur indirectly through an attack by an oxidant such as ferric ions and protons through various intermediates to sulfate ions. The ferric iron is produced by the bacterial catalysed oxidation of ferrous iron present in the mineral and re-oxidation of ferrous ions in solution by oxygen and the protons are generated by the bacteria. Sand et al., (1995, 2001) reasoned that the two proposed mechanisms can take place simultaneously during the sulfide oxidation reactions. The anticipated reactions for the two mechanisms are shown in equation [5] to [9].

Direct

$$FeS_2 + 3.5O_2 + H_2O = Fe^{2+} + 2H^+ + 2SO_4^{2-} \quad [5]$$

$$2Fe^{2+} + 0.5O_2 + 2H^+ = 2Fe^{3+} + H_2O \quad [6]$$

Indirect

$$FeS_2 + 14Fe^{3+} + 8H_2O = 15Fe^{2+} + 16H^+ + 2SO_4^{2-} \quad [7]$$

$$MS + 2Fe^{3+} = M^{2+} + S^o + 2Fe^{2+} \quad [8]$$

$$S^o + 1.5O_2 + H_2O = 2H^+ + SO_4^{2-} \quad [9]$$

Schippers and Sand (1999) postulated two leaching models for the indirect leaching mechanism depending on the sulfide mineral involved, either through the thiosulfate or the polysulfide mechanisms.

The thiosulfate mechanism is applicable to oxidation of acid-insoluble metal disulfide minerals, with a nominal sulphur oxidation state of -1, such as pyrite (FeS_2), molybdenite (MoS_2) and tungstenite (WS_2). The dissolution is through ferric iron attack, forming ferrous iron and thiosulfate as the primary sulfur intermediate. The ferric ion is regenerated by the iron oxidising bacteria and the thiosulfate is oxidised to sulfate via intermediate sulfur compounds such as tetrathionate, sulfanemonosulphonic acid and trithionate and small amounts of elemental sulfur as well as pentathionate. The overall oxidation of the sulfide to sulfate is illustrated in Figures 2.1 and 2.2 as proposed by Sand, et al., (1995, 2001). The main reactions for pyrite oxidation are given as equations [10] to [14].

$$FeS_2 + 6Fe^{3+} + 3H_2O = S_2O_3^{2-} + 7Fe^{2+} + 6H^+ \quad [10]$$

$$4Fe^{2+} + O_2 + 4H^+ \xrightarrow{\text{bacteria}} 4Fe^{3+} + 2H_2O \quad [11]$$

$$S_2O_3^{2-} + 8Fe^{3+} + 5H_2O = 2SO_4^{2-} + 8Fe^{2+} + 10H^+ \quad [12]$$

Overall reaction

$$FeS_2 + 14Fe^{3+} + 8H_2O = 2SO_4^{2-} + 15Fe^{2+} + 16H^+ \quad [13]$$

Overall reaction based on the primary oxidant is

$$2FeS_2 + 7O_2 + 2H_2O = 4SO_4^{2-} + 2Fe^{2+} + 4H^+ \quad [14]$$

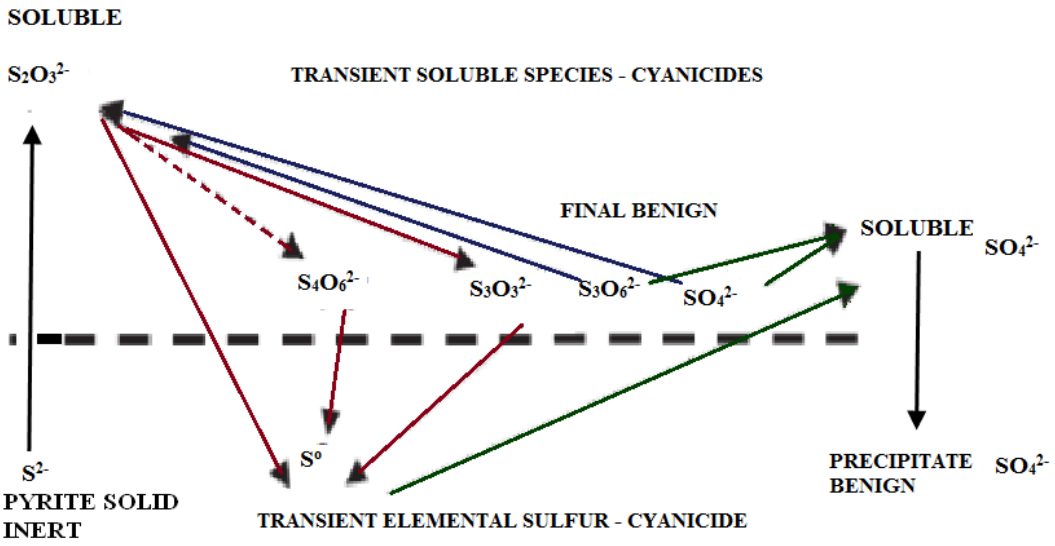

Figure 2.1. Schematic cycle for pyrite degradation (Sand et al., 1995)

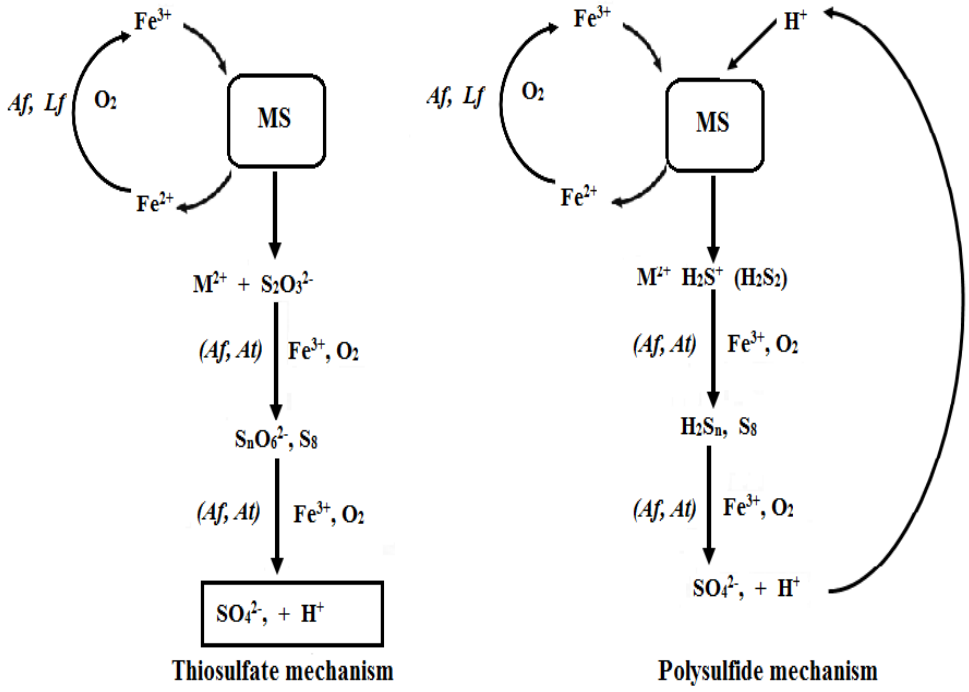

Figure 2.2. Thiosulfate and polysulfide mechanisms in bioleaching of metal sulfides. MS = metal sulfide; M^{2+} = metal ion; $S_2O_3^{2-}$ = thiosulfate; S_n^{2-} = polysulfide with a chain length (n); S_8 =elemental sulfur; Af, Lf, At = enzymatic reaction by Acidithiobacillus ferrooxidans, Leptospirillum ferrooxidans, and/or Acidithiobacillus thiooxidans; (Af, At) = enzymatic reaction possible (Sand et al., 2001)

The polysulfide mechanism is applicable to oxidation of acid-soluble metal sulfides, such as sphalerite (ZnS), chalcopyrite ($CuFeS_2$), arsenopyrite (FeAsS), galena (PbS), and hauerite (MnS_2). In this mechanism the dissolution is through the combined attack of the sulfide by the ferric ions and protons resulting in the formation of elemental sulfur as the main intermediate. The elemental sulfur is relatively stable but the bacteria can catalyse its oxidation by oxygen to the sulfate. The mechanism can be illustrated as in equations [15] to [17] (Schippers and Sand, 1999).

$$MS + Fe^{3+} + H^{+} = M^{2+} + 0.5H_2S_n + Fe^{2+} \quad (n \geq 2) \quad [15]$$

$$0.5H_2S_n + Fe^{3+} = S^{o} + H^{+} + Fe^{2+} \quad (\text{for } n = 2) \quad [16]$$

$$S^{o} + 1.5O_2 + H_2O = SO_4^{2-} + 2H^{+} \quad [17]$$

In the processing of refractory sulfidic gold ores the liberation of gold from the sulfide matrix is the most important parameter, hence, the biooxidation process may be terminated before most of the sulfur species are completely oxidised to the sulfate leaving the intermediates in the residue. These intermediate sulfur species pose a challenge during the cyanidation process where they react with the cyanide ion, thereby contributing to high cyanide demand.

2.3 Plant practice - biooxidation flow sheet

The bacterial oxidation of refractory gold ores processing plants typically incorporates crushing and milling prior to concentrate production by flotation, regrinding, bacterial oxidation of the concentrate, solid-liquid separation (counter current decantation washing circuit), and solution neutralisation followed by cyanidation and gold recovery from the oxidised residue. The generic flowsheet is illustrated in Figure 2.3 and the BIOX® process flowsheet in Figure 2.4.

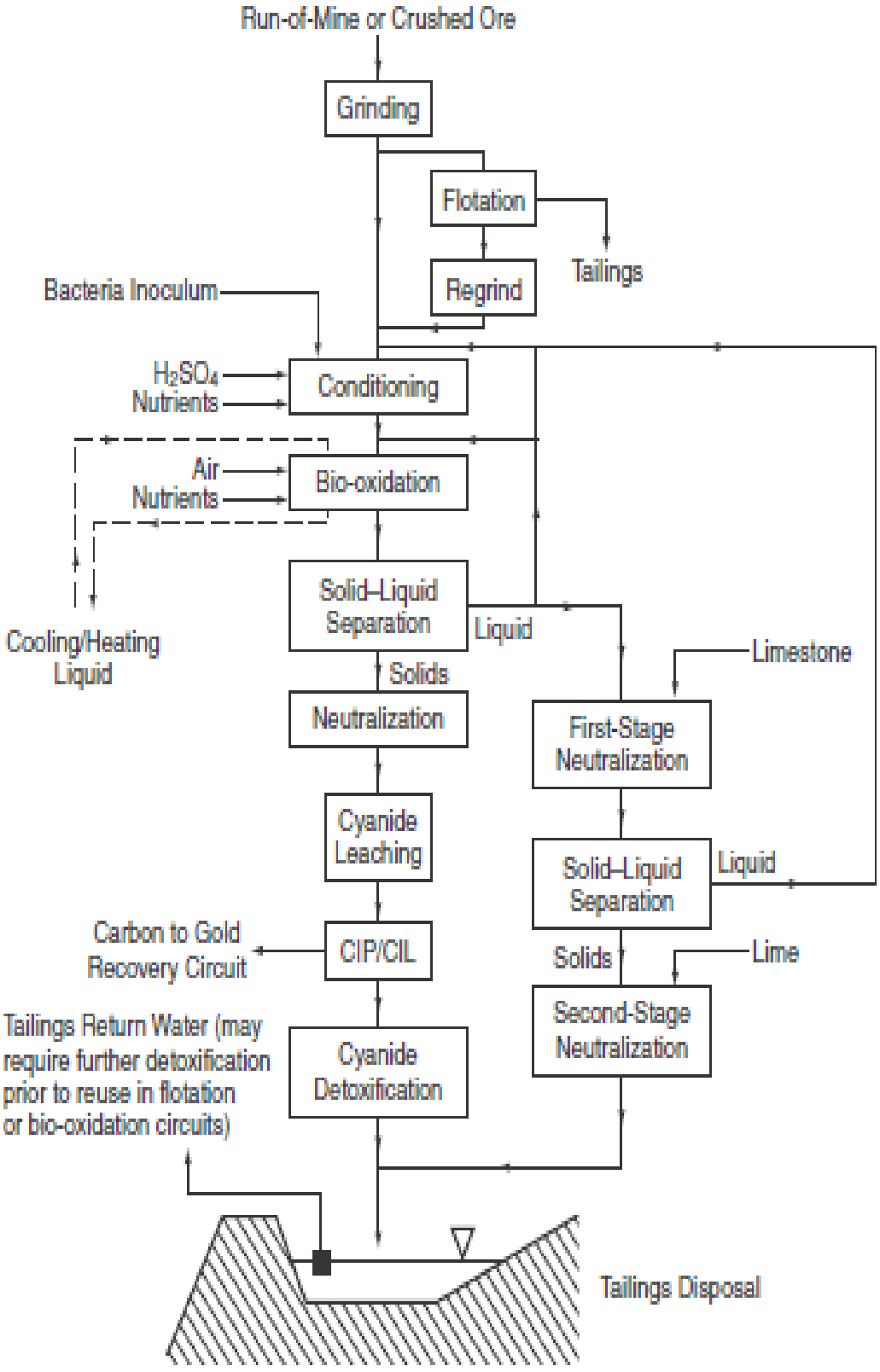

Figure 2.3. Schematic flowsheet for biological oxidation of gold sulfide ore (Marsden and House, 2009)

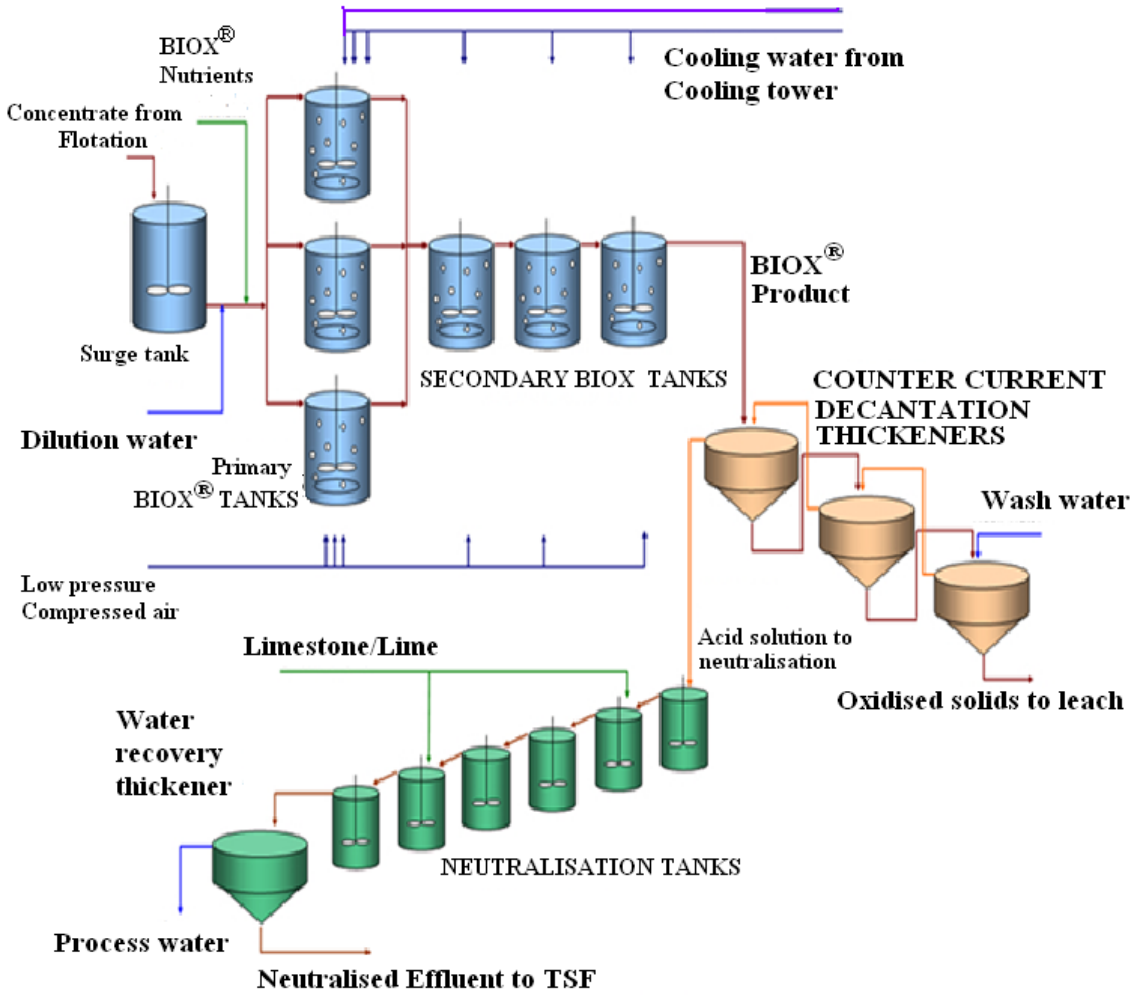

Figure 2.4. Typical BIOX® process flowsheet (Biomin)

The sulfide–sulfur content in the feed to the agitated tank bacterial oxidation process is critical for adequate bacterial growth and activity during biooxidation. In most operations a flotation pre-concentration step is employed to optimise the sulfur content of the feed to ensure effective operation of the process. Typically in conventional biooxidation flowsheets the feed to the reactors is divided equally between three primary reactors, and the partially oxidized product exiting from the primary reactors is recombined and enters three secondary reactors operating in series. This gives the primary reactors sufficient residence time to allow the bacteria to grow and divide and double its population so as to increase the sulfide-sulfur oxidation efficiency. The bacterial population in the secondary reactors would have been optimised, thus shorter

retention times are possible, with about half that required in the primary reactors acceptable to complete sulfide-sulfur oxidation.

The concentrate feed for bacterial oxidation is generally diluted with addition of water to typical pulp densities of 15 to 20 mass percent solids concentration in agitated aerated tanks. The pulp retention time in the biooxidation reactors depends on the oxidation rates required, and is a function of the sulfide-sulfur content, its reactivity, grind size, and mineralogical composition of the concentrate and typically takes 4 to 6 days (van Aswegen et al., 2007). Investigations by Komnitsas and Pooley (1990) indicated that arsenopyrite is more reactive than pyrite, thus its oxidation rate is faster than that of pyrite, resulting in ores where gold is locked in arsenopyrite requiring a shorter residence time than those where the gold is locked in pyrite. In agitated tank systems ore particle size is generally limited by the down-stream processes such as solid liquid separation and also the requirements for the cyanide leaching process. Typically particle sizes similar to those used for cyanide leaching processes are used for feed concentrates, 80% < 75 µm (Dew et al., 1997).

The biooxidation residues contain dissolved ions, which are typically removed by washing through a three stage counter current decantation (CCD) circuit to promote gold recovery and reduce cyanide consumption during the cyanidation process. The overflow liquor of the CCD wash is neutralised in a three-stage process to pH 7 to 8 to produce stable precipitates containing the iron and arsenic which are safe for disposal on a tailings dam (van Aswegen et al., 2007).

2.4 Optimisation of bioleaching/biooxidation

The oxidation rate and efficiency of the sulfide-sulfur during the bioleaching process depends on a number of physicochemical and microbiological factors that affect the growth and activity of the bacteria. These parameters must be maintained within a certain range for each type of bacteria to optimise growth and activity and achieve oxidation of the sulfide mineral. The parameters of prime importance for control and optimisation of sulfide ores/concentrates include temperature, acidity, mineralogical composition of the ore, oxidising conditions, availability of nutrients, oxygen and carbon dioxide, surface area, solid ratio, and concentration of toxic ions (Deveci et al., 2003; Akcil and Deveci, 2010).

Each type of bacteria is active within certain pH ranges, with their activity, and growth and consequently the sulfide oxidation reduced outside this pH range. Hence, the acidity of bioleaching media must be controlled within the optimum pH for effective operation. Acidophilic bacteria are active within the pH range of 1.5 to 2.5. However, in practice the operating pH is often lower than the optimum values for growth, e.g. pH 1.2 to 1.8 for the BIOX® process and pH 1.3 to 1.5 for the BacTech process to minimise the formation of undesirable ferric precipitates, such as jarosites. The formation of precipitates result in the removal of the oxidising ferric iron that causes the indirect leaching of minerals from the solution and also the transfer of labile iron and sulfur species to the cyanidation process in the case of gold leaching (Brierley and Briggs, 2002). In most operations the pH in the slurry is controlled by the addition of limestone and sulfuric acid in the reactors.

The dissolved oxygen plays a vital role in the biooxidation process of sulfide ores where the molecular oxygen is used as the terminal electron acceptor in aerobic conditions. Sun et al., (2012) reported that the microbial growth and the biooxidation rates increased with the dissolved oxygen concentration. Oxygen is typically supplied to the reactors by low pressure injection with a dissolved oxygen concentration of more than 2 milligrams per litre required at all times in the slurry (van Aswegen et al., 2007).

The bacteria involved in the biooxidation of sulfide minerals are chemolithoautotrophic species and use carbon dioxide from the atmosphere as their carbon source for the synthesis of new cell material (Bosecker, 1997). The level of carbon dioxide in the biooxidation primary reactors is also augmented by the addition of carbonate in the form of limestone to the concentrate to ensure that sufficient CO_2 is available to promote bacterial cell production.

For effective growth and activity of most bacteria used in the biooxidation process certain levels of nutrients are required for cell mass production and energy for biosynthesis and maintenance. Most ores processed may contain nutrient concentrations that are below the minimum nutrient levels required for optimum bacterial activity; hence supplementary nutrients must be added. In most operations nutrients are added in the primary reactors in the form of nitrogen, phosphorous and potassium in various forms which include fertilizers and salts with the quantities added varying with the composition of ore being processed. The standard addition rates and nutrient sources

specified by Gold Fields and the nutrient addition at Fairview BIOX® plant for 1987, 1988, and 1989 are listed in Table 2.1 (van Aswegen et al., 1989, 2007).

Table 2.1. Nutrient addition for the BIOX® process (van Aswegen et al., 1989, 2007)

	Fairview BIOX Plant			Standard addition rates
	1987	1988	1989	
NH_4^+ (kg/t)	9.62	8.73	8.40	2.19 (1.7 as N)
K^+ (kg/t)	13.05	4.27	1.43	0.90
PO_4^{3-} (kg/t)	1.50	1.52	1.56	0.92 (0.3 as P)

In agitated tank biooxidation reactors agitation plays a critical role by enhancing the mass transfer rates of gaseous phase oxygen and carbon dioxide to the liquid phase, transfer of heat to or from the medium, and to achieve homogeneity for the gas-liquid-solid system and hence to maintain suitable growth conditions for bacteria by minimising the development of gradients of concentration, temperature and pH throughout the reactor system. Increasing the agitation intensity may result in an improvement in the mass transfer rates of gaseous phases to the liquid phase and accelerate the dissolution of minerals in bioreactors. However, d'Hugues et al., (1997) pointed out that the exposure of microorganisms to a strong shear atmosphere could result in the destruction of cells, the inhibition of biomass growth or product synthesis, the change in morphology, the thickening of the cell wall, and the hindrance of the attachment of bacteria to the solid substrate, leading to a reduction in microbial growth and activity. Deveci (2002) observed that the performance and growth rate of bacteria were sensitive to agitation rate and the solids density and decreased with agitation intensity and solids content.

The bacterial leaching of sulfide minerals occurs through surface chemical reactions through leaching by bacterially generated ferric iron and/or acid or attachment of bacteria. An increase in the surface area exposed for leaching through size reduction results in a higher rate of extraction. In practice the particle size used for processing refractory gold concentrates in agitated tank reactors is 80% < 75 µm. The available surface area for bacterial leaching is also dependent on the pulp density employed with higher pulp densities giving more surface area for leaching. In agitated tank reactors the maximum pulp density employed is 20 mass percent due to a number of undesirable

effects. The use of high pulp density results in decreases in the bacteria-to-solid ratio, and the availability of nutrients, oxygen and carbon dioxide, and also in mechanical damage to microbial cells by solids, as well as the inhibitory effect of increasing metal ion concentrations in solution (Deveci, 2002).

Each type of bacterial microorganism thrives most efficiently in a relatively well defined temperature range where its oxidising activity is optimum. The decrease in the oxidative activity of the bacteria beyond the optimum temperature may be attributed to the likely denaturation of the proteins involved in the oxidising system of the bacteria. The sulfide oxidation reactions that occur during the biooxidation process are exothermic in nature resulting in an increase in the temperature of the pulp. To maintain a set temperature for optimum bacterial activity and realise maximum sulfide oxidation the reactors are continuously cooled with circulating water.

2.5 Formation of secondary ferric minerals

In bacterial leaching systems, the bioorganisms catalyse the oxidation of ferrous iron in the presence of oxygen to the ferric iron consuming hydronium ions, as indicated in equation [18].The ferric iron is in turn used to oxidise the sulfide minerals. However, the acidic sulfate-rich environment used in biooxidation also favours the precipitation of the ferric iron from the system, as iron hydroxysulfate minerals such as the jarosite-group minerals ($MFe_3(SO_4)_2(OH)_6$), schwertmannite ($Fe_8O_8(OH)_6(SO_4).nH_2O$, and scorodite ($FeAsO_4$), via equations [1], [19] and [20], with associated acid generation. The dissolution of carbonates from the ore releases calcium which precipitates as gypsum, as shown in equation [21]. Gramp et al., (2008) reported that the properties and the phases of ferric iron precipitates produced are dependent on the ionic composition (ferric iron, sulfate, and alkali cations) and concentration of the medium, temperature, contact time, and pH. The formation of secondary precipitates was also argued by Tanaka et al., (2015) to result in the consumption of ferric iron used as the oxidant in sulfide oxidation, and the precipitates also tend to conceal mineral sites on ore particles hindering biooxidation/bioleaching efficiencies.

$$4Fe^{2+} + O_2 + 4H^+ \xrightarrow{\text{bacteria}} 4Fe^{3+} + 2H_2O \quad [18]$$

$$8Fe^{3+} + SO_4^{2-} + 14H_2O = Fe_8O_8(OH)_6(SO_4)_{(s)} + 22H^+ \quad [19]$$

$$2H_3AsO_4 + Fe_2(SO_4)_3 = 2FeAsO_{4(s)} + 3H_2SO_4 \quad [20]$$

$$CaMg(CO_3)_2 + 2H_2SO_4 = CaSO_{4(s)} + MgSO_{4(s)} + 2CO_2 + 2H_2O \quad [21]$$

Studies by Bigham et al., (1996), demonstrated that jarosite (K, Na, $H_3O(Fe_3(OH)_6(SO_4)_2)$ may be formed at pH < 3 at high sulfate concentrations, while schwertmannite ($Fe_8O_8(OH)_6SO_4$) is the dominant deposit in the pH range 3 to 4.5. At higher pH values (pH > 6.5) ferrihydrite ($Fe_5HO_8.4H_2O$) and goethite (α-FeOOH) have been demonstrated to be the dominant compounds. The availability of alkali cations or ammonium ions in the media promotes the formation of jarosite minerals as illustrated in equation [1] ahead of schwertmannite as they occupy the M position in the jarosite minerals. Thus, the concentration of the alkali cations or ammonium ions in the media will influence the type of product formed with low concentrations favouring the formation of schwertmannite. Various authors reported schwertmannite to be the dominant product at low alkali concentrations even at pH values as low as 1.9, and at higher single or combined concentrations of alkali ions, yellowish jarosite phases were the main products (Wang et al., 2007; Jones et al., 2014; Jin-yan et al., 2009). Dutrizac (2008) reviewed the formation of jarosites and indicated that potassium ions greatly facilitate the formation of a jarosite phase, with the rate of precipitation of potassium jarosite faster than that of ammonium jarosite, sodium jarosite, or hydronium jarosite under comparable synthesis. To discourage the precipitation of jarosite minerals, Jansen and Webb (1995) recommended the reduction or elimination of cations that form stable hydroxysulfates, especially K^+, in the nutrient solutions employed with low pH bioreactors.

Babcan (1971) clarified the relationship between the temperature and pH for the formation of potassium jarosite in the temperature range 20 to 200ºC as illustrated in Figure 2.5. The stability zone of jarosite was observed as a band sloping to lower pH with increasing temperature. The formation of jarosite is favoured at higher temperatures even at lower pH values. The stability region extends from pH 2 to 3 at 20ºC, from pH 1 to 2.3 at 100ºC, and from pH 0 to 1.2 at 200ºC. At pH values below the stability region, no precipitate is formed and at higher pH values, various other iron compounds are produced. The temperature and pH also impact on the kinetics of the precipitation process due to their influence on supersaturation. However, the stability regions are also influenced by the concentration of ions present in solution.

Dutrizac and Chen (2010) and Bigham et al., (2010) reported that the synthesis temperature also affects the formation and final elemental composition of the jarosite phases formed. The phosphorous and sulfur content in the jarosite was observed to increase with synthesis temperature whilst the potassium content decreased with temperature for jarosite synthesised in an acidic sulfate matrix in the absence of iron oxidising bacteria. Bigham et al., (2010) also established that the potassium, sodium and ammonium jarosites can be synthesised at ambient temperatures, whereas the hydronium end-member usually requires elevated temperatures in excess of 95ºC, although it partially substitutes for other monovalent cations in the M position of biogenic jarosite precipitates formed under ambient conditions.

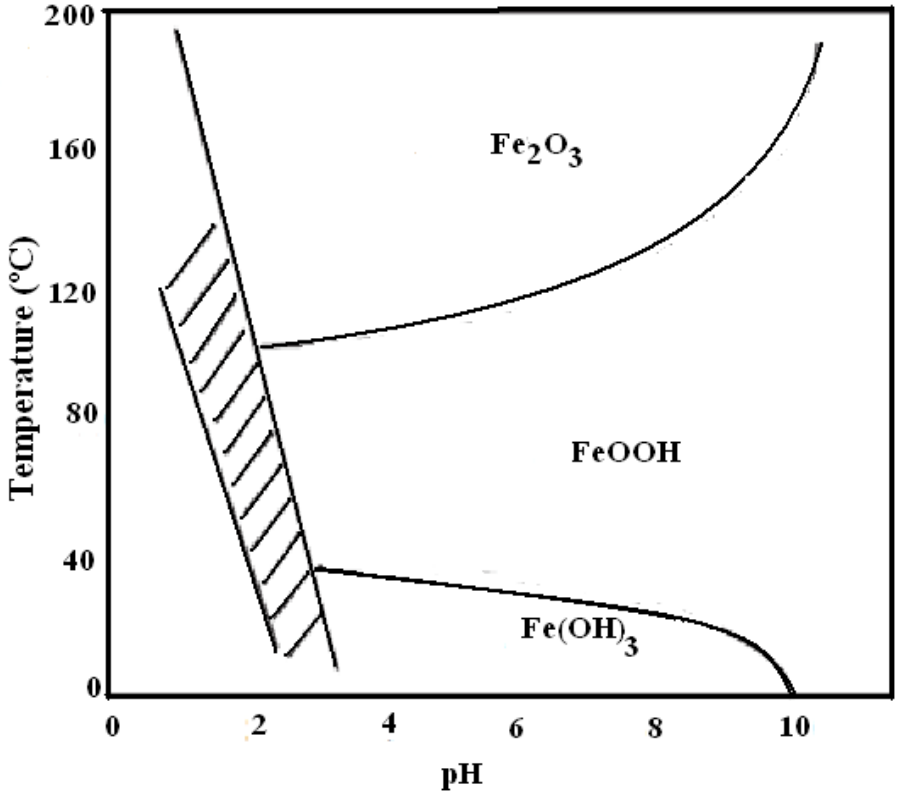

Figure 2.5. Stability field for potassium jarosite formation (hatched area) as a function of pH and temperature for jarosite formation from 0.5M $Fe_2(SO_4)_3$ solution at 20 to 200ºC (Babcan, 1971)

2.6 The behaviour of impurities during jarosite precipitation

Jarosite precipitates typically sorb and co-precipitate considerable amounts of elements such as Pb, As, Ag, or even Zn, Cu, Co, etc. Dutrizac (1984) observed that the divalent base metals do not significantly precipitate into the jarosite structure and the order of co-precipitation was found to be as shown below:

$Co^{2+} > Cu^{2+} > Ni^{2+} > Zn^{2+} > Mn^{2+} > Cd^{2+} > Mg^{2+}$

Trivalent ions including Al^{3+}, Ga^{3+}, In^{3+} and Cr^{3+} were also found to substitute for Fe^{3+} in the jarosite formula. It was also pointed out that the amount of divalent cations incorporated into the jarosite structure increased with their concentrations. In this regard the jarosite may act as a temporary sink for trace metals which are released when the jarosite dissolves.

2.7 Dissolution of minerals in acidic and alkaline solutions

2.7.1 Mechanism of dissolution

Dissolution reactions in a solvent such as water may take place through a mechanism whereby the less stable phase dissolves and a more stable is formed and if insoluble precipitates from the fluid phase. The driving force for dissolution (and all chemical processes) is determined by the Gibbs free energy change. The reaction interface is associated with a thin fluid film at the interface between the parent and product phases. The dissolution of minerals takes place through three discrete steps: diffusion of reactants to the mineral surface, a reaction at the mineral surface followed by diffusion of ions from the mineral surface to the bulk solution.

The dissolutions of solids can be classified as oxidative/reductive, those that involve a change in oxidation state of one or more species, and non-oxidative dissolution when the formal oxidation states of the solute species are identical both in the solution and in the solid state. In the non-oxidative reactions, such as the dissolution of oxides, the rate of dissolution is mainly dependent on the pH which indicates that the H^+ ion (or alternatively OH^- ion) is primarily responsible for dissolution, as well as the concentration of anions (or ligands) which might form complexes with the metal ions (Nicol and Scott, 1979). Metal cations in aqueous solution are aqua complexes with

most metal ions coordinating to four to six H_2O molecules per ion (Stumm and Morgan, 1996).

2.7.2 Jarosite decomposition

Jarosites ($MFe_3(SO_4)_2(OH)_6$) are ionic minerals and their dissolution in aqueous media is non-oxidative, and only involves the breakdown and formation of new bonds. The jarosite dissolution rate is affected by the pH, stability of the decomposition products, mainly Fe^{3+} in solution, the stability of ferric mineral phases, and the formation of passivating ferric mineral films on the reacting mineral surface. The ionic strength of the solution also has an effect on the thermodynamics and kinetics of jarosite dissolution. On decomposition cations in the M site (H_3O^+, K^+, Na^+, NH_4^+) and SO_4^{2-} are preferentially leached from the mineral surface and all minor elements incorporated during precipitation become solubilised and disperse. Secondary iron oxide/hydroxide minerals represented by $Fe(OH)_3$, with the specific phase likely dependent on pH and the rate of formation, are precipitated, and coating of jarosite by such material is likely responsible for inhibiting subsequent jarosite dissolution. Welch et al (2008) reported that the dissolution rates for natural mineral jarosites were 1 to 3 orders of magnitude slower than the synthetic jarosite samples, suggesting that residual solids and presence of other minerals were inhibiting reaction relative to the clean synthetic jarosite. The dissolution rates of jarosites were observed to increase with increase in either H^+ or OH^- in solution. Different dissolution mechanisms for acidic and alkaline conditions were suggested by Welch et al., (2008) with potassium jarosite dissolving in acidic conditions forming soluble ionic species, consuming acid, and producing ferric iron as the reaction proceeds via equation [22] and with the rate increasing with acidity. For less acidic to alkaline conditions, i.e. pH > 3 to 4, potassium jarosite dissolves forming soluble ionic species and solid species consuming hydroxide during the reaction and the reaction rate increases with an increase in pH and an iron–rich secondary phase is formed, as indicated for reaction [23] below. The two mechanisms results in a “U” shaped trend in dissolution rates with pH, with the transition between the two mechanisms occurring at approximately pH 3.7 as depicted in Figure 2.6.

$$KFe_3(SO_4)_2(OH)_{6(s)} + 6H^+ = K^+ + 3Fe^{3+} + 2SO_4^{2-} + 6H_2O \quad [22]$$

$$KFe_3(SO_4)_2(OH)_{6(s)} + 3OH^- = K^+ + 3Fe(OH)_3 + 2SO_4^{2-} \quad 23]$$

The hydrolysis of ferric ions in aqueous solutions is dependent on time, temperature and in particular pH as the parameters that govern the transformation into crystalline phases. The ageing process may be divided into several steps (a) primary hydrolysis giving rise to low-molecular weight complexes (mono- and dimer) i.e. $Fe(OH)^{2+}$, $Fe(OH)_2^{+}$, $Fe_2(OH)_2^{4+}$, (b) formation and aging of polynuclear polymers i.e. $Fe_n(OH)_m(H_2O)_x^{(3n-m)+}$ or $Fe_nO_m(OH)_x^{(3n-2m-x)+}$, (c) precipitation of ferric oxides and hydroxides, i.e. ($Fe(OH)_3$, FeOOH and Fe_2O_3 (Dousma and de Bruyn, 1978).

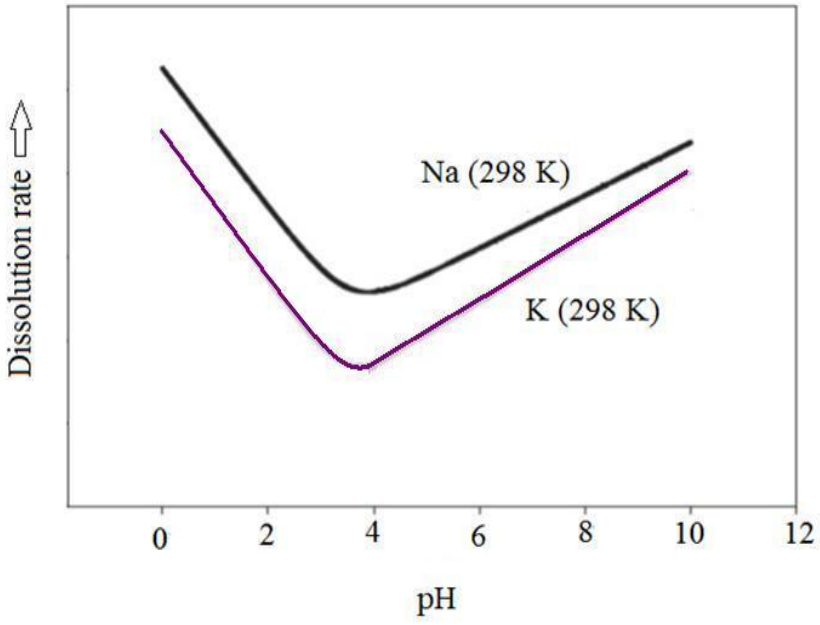

Figure 2.6. Schematic representation of jarosite dissolution rates for sodium (Na) and potassium (K) jarosites, respectively (Madden, et al., 2012)

The kinetics of the alkaline decomposition-cyanidation of synthetic jarosites has been studied extensively by several authors, inter alia ammonium jarosite (Salinas, et al., 2001), argentojarosite (Roca, et al., 1993), argentian natrojarosite (Patino, et al., 1998), argentian ammonium jarosite (Patino, et al., 2003), sodium arsenojarosite (Patino, et al., 2013), silver ammonium jarosite (Roca, et al., 2006). In all cases it was stated that the process occurs via two steps in series, a slow step of alkaline decomposition, which involves the breaking of bonds which typically controls the overall rate of the process, followed by a fast step of complexation of the decomposition products. During the first step, which typically includes an induction period during which the yellow colour of the jarosite shows no change, and the levels of sulfate ions remained at trace levels in the solution, after which the actual transformation and dissolution occurs with the colour of

the solid changing from yellow to reddish and the level of sulfate ions in the solution increasing progressively. During this stage the ions (SO_4^{2-}, K^+, Fe^{3+}, and OH^-) are removed from the lattice and the iron will form the hydroxide while the other ions are solvated to form hydrated ions as illustrated in equation [23].

If the jarosite contains other cations (e.g. silver or base metal cations of copper, nickel and cobalt) in its structure which might have been incorporated during precipitation, these may also precipitate out as hydroxides, as indicated for silver in equation [24].

$$Ag^+ + 2OH^- = Ag(OH)_{2(s)} \quad [24]$$

In the presence of other ligands in the media, for example cyanide, these cations will also react with them to form cyanide complexes and pass into the solution for example via equations [25] – [27];

$$Fe^{3+} + 6CN^- = Fe(CN)_6^{3-} \quad [25]$$

$$Ag^+ + 2CN^- = Ag(CN)_2^- \quad [26]$$

$$Cu^+ + 4CN^- = Cu(CN)_4^{3-} \quad [27]$$

The equilibrium of the dissolution reaction is driven to the right due to the formation of very stable reaction products, e.g. $Fe(OH)_{3(s)}$ and $Fe(CN)_6^{3-}$, to favour the dissolution of the jarosite. The formation of cyanide complexes will be favoured at higher pH values as the hydrolysis of cyanide will decrease and more cyanide will be available for complexation, as indicated for iron complexes in Figure 1.2.

In the presence of strong ligands such as carboxylic acids, e.g. ethylenediaminetetraacetic acid (EDTA), nitrilotriacetic acid (NTA), oxalic acid, tartaric acid, acetic acid, lactic acid, and citric acid, the solubility of ferric hydroxysulfates in aqueous solutions is increased by forming strong ferric complexes (Pachla et al., 1991; Martel and Smith, 1989). The leaching of silver sulfide with thiosulfate catalysed by ferric iron complexes was studied using ferric-EDTA, ferric-oxalate and ferric citrate and no iron precipitation was observed during leaching. The activity of ferric iron is reduced by complexation and the precipitation of iron hydroxides, which may also passivate the ore, is then avoided (Miller and Brown, 2005).

2.8 Solution chemistry of cyanide

The cyanide ion (CN^-) is a singularly charged anion consisting of one carbon atom and one nitrogen atom joined with a triple bond. The cyanide anion can exist in solution as hydrocyanic acid (or hydrogen cyanide, $HCN_{(aq)}$) or as free cyanide anion ($CN^-_{(aq)}$) depending on the pH of the solution. $HCN_{(aq)}$ is a relatively weak acid with a pKa of 9.24 at 25 °C which dissociates according to equation [28]. The dissociation reaction equilibrium as a function of pH is graphically displayed in Figure 2.7 (Sharpe, 1976). At low pH values HCN is the dominant species and has a vapour pressure of close to one atmosphere at ambient conditions with the result that cyanide may be lost due to volatilisation as $HCN_{(g)}$. This may contribute to the high consumption of cyanide in gold leaching processes if the pH is not controlled at relatively high values. The gold extraction process is typically carried out at a pH ≥ 10.5, as at this pH most of the cyanide in the solution is in the form of the cyanide anion (CN^-) and losses to the gas phase limited.

$$HCN_{(aq)} = H^+ + CN^- \quad (pKa = 9.24 \text{ at } 25°C) \quad [28]$$

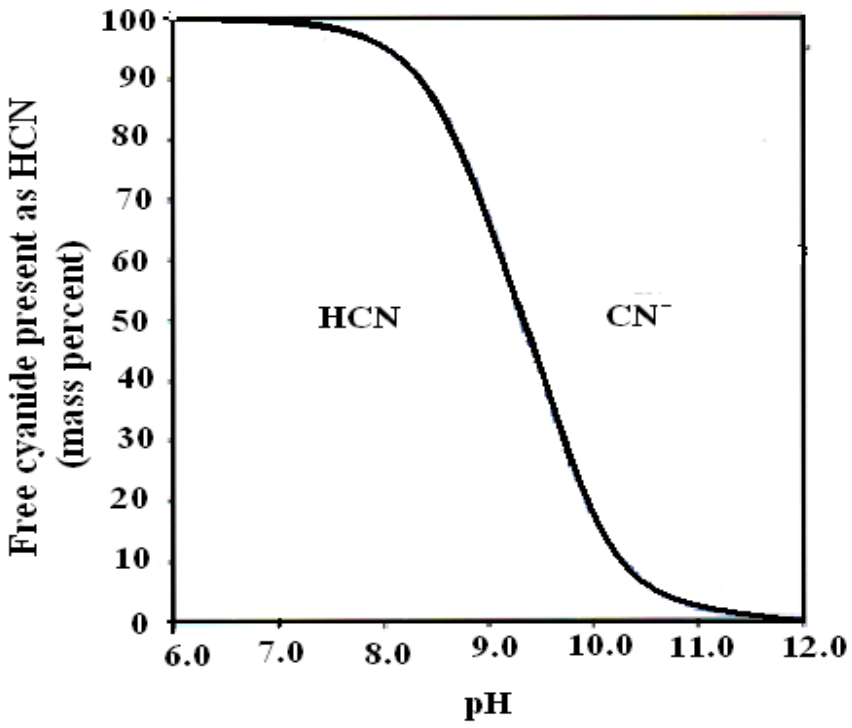

Figure 2.7. Distribution of the cyanide anion (CN^-) and molecular hydrogen cyanide (HCN) as a function of pH (25 °C) (Sharpe, 1976)

The cyanide anion is a versatile ligand that reacts with many metal species, mainly transition metals, in a step-wise manner to form anionic metal-cyanide complexes with general formula $M(CN)_x^{n-x}$, where M is a metal cation, x is the number of cyanide groups, and n is the ionic charge of the metal, as indicated in equation [29]. The stabilities of these complexes vary with the metal ion and requires moderate to highly acidic conditions in order to dissociate. The metal-cyanide complexes are typically classified according to the strength of the bonding between the metal and the cyanide ion into two groups, namely weak acid dissociable (WAD) metal-cyanide complexes ($\log K \leq 30$) and strong acid dissociable (SAD) metal cyanide ion complexes ($\log K > 30$). The WAD metal-cyanide complexes are those in which the cyanide ions are weakly bonded to the metal cation, such that they can dissociate under mildly acidic conditions (pH = 4 to 6) to produce free cyanide. The SAD metal-cyanide complexes require strong acidic conditions (pH < 2) in order to dissociate and are thus much more stable in aqueous cyanide solutions than the weak ones (Marsden and House, 2009).

$$M^{n+} + xCN^- = M(CN)_x^{(n-x)-} \quad [29]$$

From the cyanide-metal dissociation pH values it follows that all the metal-cyanide complexes are stable in the pH range used in the cyanidation of gold ($pH \geq 10.5$), hence they all contribute to cyanide consumption under these conditions. The metal-cyanide complexes may also form double salt-type compounds with alkali or heavy metal cations in the alkaline cyanide conditions. The ferrocyanide complex ($Fe(CN)_6^{4-}$) which is common in gold leaching, forms a large number of metal salts of varying solubility (Wang and Forssberg, 1990). The cyanide can also be lost by adsorption of the cyanide anion and metal-cyanide complexes on organic and inorganic constituents such as oxides of aluminium, iron and manganese, certain types of clays, feldspars and organic carbon. The cyanide anion can also react with elemental sulfur and labile sulfur species such as the free sulfur, thiosulfate, and polysulfides, to form thiocyanate (SCN^-) via equations [30] to [32]. The mechanisms for the biooxidation of sulfide minerals, such as pyrite, chalcopyrite, chalcocite, pyrrhotite, and arsenopyrite, discussed earlier, indicated that a number of sulfur species may serve as intermediates during sulfide dissolution, as already illustrated in Figure 2.2, which may contribute to cyanide consumption during gold cyanidation.

$$S + CN^- = SCN^- \quad [30]$$

$$S_xS^{2-} + CN^- = S_{x-1}\,S^{2-} + SCN^- \quad [31]$$

$$S_2O_3^{2-} + CN^- = SO_3^{2-} + SCN^- \quad [32]$$

In the presence of strong oxidising agents such as ozone (O_3), hydrogen peroxide (H_2O_2), or hypochlorous acid (HOCl) free cyanide and hydrogen cyanide may also be oxidised to form cyanate (CNO^-) via equations [33] to [34] or, depending on the pH, the protonated form HOCN (pK_a = 3.45 at 25°C). This reaction is extremely slow using oxygen, but can be enhanced by the action of ultraviolet light, heat, bacteria, and catalysts such as titanium dioxide, zinc oxide, and cadmium sulfide.

$$2CN^- + O_2 = 2CNO^- \quad [33]$$

$$2HCN + O_2 = 2CNO^- + 2H^+ \quad [34]$$

The cyanate once formed may also be hydrolysed to ammonia and carbon dioxide as shown in equation [35] with the rate relatively rapid in acidic conditions as the products do not accumulate in solution.

$$CNO^- + 2H_2O = CO_2 + NH_3 + OH^- \quad [35]$$

At higher pH values, especially above 9, free ammonia is the dominant ammoniacal species which forms soluble amine complexes with heavy metals such as copper, zinc, and nickel inhibiting their precipitation as metal hydroxides (Kuyucak, 2001). The ammonia formed may be further chemically or biologically oxidised to nitrate as the end-product of cyanide oxidation.

2.9 Cyanidation for the recovery of gold

Gold is a noble metal and is inert to most chemical reactions in aqueous solutions, including acids in non-complexing media. Thermodynamically gold ions (aurous or auric) are not stable in aqueous systems as they are reduced by the water to the metallic gold. To solubilise the gold into solution a complexing ligand, which stabilises the gold in solution, as well as a suitable oxidising agent are required. The typical ligand for gold extraction is cyanide (CN^-) which is greatly effective for gold and silver dissolution and has a relatively low cost. Oxygen (O_2) supplied from air is the typical oxidising agent used in cyanide leaching in alkaline media. The gold is oxidised to Au(I) and dissolves

to form the cyano complex ($Au(CN)_2^-$); the $Au(CN)_4^-$ complex is also formed, but the Au(I) complex is more stable than the Au(III) complex as shown in Figure 2.8.The process of extracting gold from ore under these conditions is called cyanidation and is chemically expressed by Elsner's equation [36] (Nicol, et al., 1987; Marsden and House, 2009)

$$4Au + 8CN^- + O_2 + 2H_2O = 4Au(CN)_2^- + 4OH^- \quad [36]$$

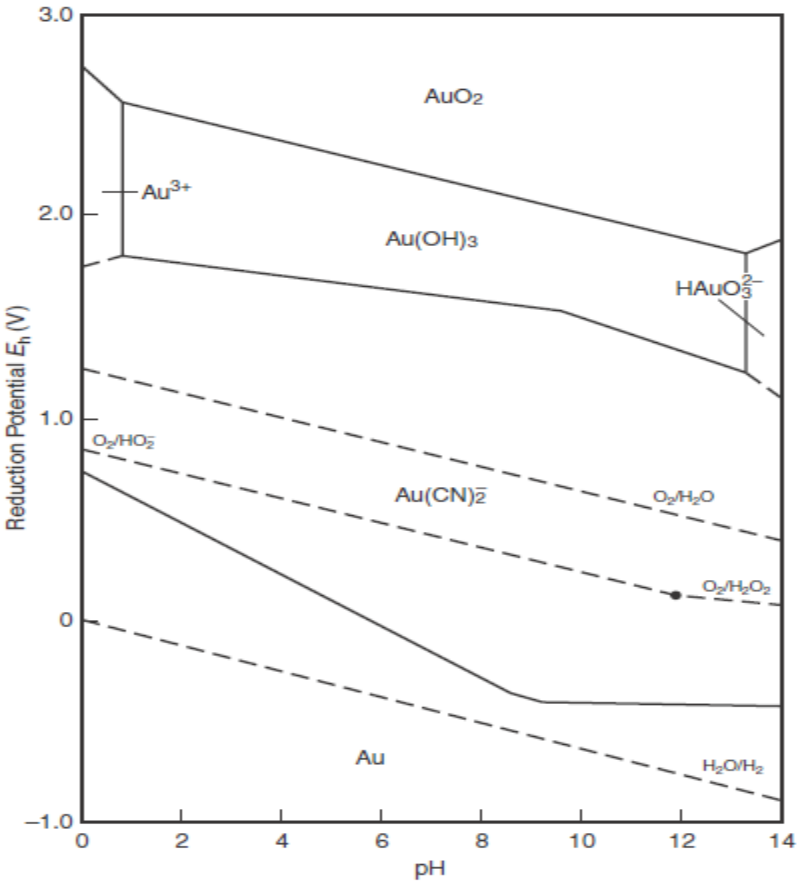

Figure 2.8. Potential-pH equilibrium diagram for the system Au-H_2O-CN^- at 25°C. Concentration of all soluble gold species =10^{-4}M $[CN^-]_{total}$ = 10^{-3}M, pO_2 = pH_2 = 1atm (Marsden and House, 2009)

From Elsner's equation the efficiency of the reaction depends on both the concentration of cyanide and oxygen, and a deficiency in one or both reduces the leaching rate and may lower the recovery in gold processing plants. In operating plants cyanide concentration is added in excess and the dissolution rate of gold will be determined by the dissolved oxygen concentration in the pulp which is also dependent on the temperature and pressure that the process operates under.

The mineralogical composition of gold ores vary depending on their origin and also determines the performance of all chemical and physical processes involved in the extraction of gold. Many metal sulfides are susceptible to dissolution and oxidation in aerated, dilute alkaline cyanide solutions, to form various sulfur containing species, including thiocyanate, thiosulfate ions, and metal ions (e.g. Fe^{2+}, Fe^{3+}, Zn^{2+}, Cu^{2+}, Mn^{2+}) which form cyano complexes as indicated by equation [37]. Thus the demand for oxygen and cyanide during cyanidation will not be limited to gold alone, interaction with other minerals and species significantly increased the cyanide and oxygen consumed (Kondos, et al., 1995; Marsden and House, 2009)

$$2MS + 2(x+1)CN^- + O_2 + 2H_2O = 2M(CN)_x^{(x-2)-} + 2SCN^- + 4OH^- \quad [37]$$

The extraction of gold is also affected by other factors such as temperature, pH and size of the ore particles.

3 EXPERIMENTAL

3.1 Overview

The first part deals with the synthesis and characterisation of potassium jarosite at conditions simulating the mesophile BIOX® process, dissolution of the jarosite in alkaline and alkaline-cyanide solutions, speciation of dissolution products, and the kinetics of jarosite dissolution. The removal of ferric iron from jarosite by pre-leaching in carboxylic acids and stabilising of jarosite decomposition products by preconditioning in alkaline aqueous solution before cyanidation were also assessed. The second section deals with the cyanidation of BIOX® residues (mesophile and thermophile) from Fairview mine (Barberton mines) to establish the stability and contribution of the jarosite to the consumption of cyanide.

3.2 Reagents

Analytical reagent grades and de-ionised water were supplied by Merck.

3.3 Synthesis and reactivity of jarosite in alkaline media

3.3.1 Jarosite precipitation

Jarosite was produced following the method by Bigham et al., (2010) at a temperature of 45^{o}C, using the mineral formulation indicated in Table 3.1.

Table 3.1. Mineral salt formulation used for jarosite precipitation

Salt	K_2HPO_4	$MgSO_4 \cdot 7H_2O$	$Ca(NO_3)_2$	$(NH_4)_2SO_4$	$Fe_2(SO_4)_3 \cdot 9.5H_2O$
(g/L)	4.35	0.50	0.01	4.00	46.00

The precipitation was done in a stirred glass reactor with the temperature controlled at 45^{o}C using a water bath. All the mineral salts were dissolved in deionised water except in the case of the ferric salt where the pH of the water was first adjusted to 1.4 using 2M H_2SO_4 before adding the ferric sulfate. Conditions favourable for jarosite precipitation were then created by slowly adjusting the pH to 2.2 by titrating with 2M KOH. The pH was measured using a Crison Basic 20 meter with an epoxy body Sintex 42 pH combination electrode. The high potassium ion concentration was used to promote the formation of the potassium jarosite and prevent the formation of schwertmannite which will be favoured when there is a deficiency of monovalent cations. The solution was

stirred at 280 revolutions per minute for 1 hour, using a Heidolph RZR 250 stirrer. The precipitate was left to age for five days unstirred in a water bath at 45ºC in 2 litre bottle, and was then filtered through Whatman No.1 filter paper and washed with distilled water. The wet jarosite was used in the dissolution experiments. Powder samples for X-ray diffraction (XRD) and X-ray fluorescence (XRF) analyses were prepared by drying in air to obtain a lumpy amber-yellow precipitate that was gently disaggregated in a mortar and pestle. The chemical composition of the precipitate was determined by dissolving it in HCl, followed by analyses using inductively coupled plasma optical emission spectroscopy (ICP-OES) with matrix-matched standards. The particle size distribution (volume based) was done on the wet sample using six runs on a Malvern Mastersizer 2000.

3.3.2 Jarosite alkaline decomposition and cyanidation

The alkaline decomposition of the jarosite was investigated by exposing it to an alkaline solution at 25ºC for 24 hours. 7.0 g (~3.0 g dry basis) of wet jarosite was suspended in500ml water with a pH of 10.5 to 11 adjusted using CaO, while stirring at 300 revolutions per minute. A sample of the wet jarosite was air dried to determine the moisture content of the jarosite and the mass adjusted to a dry basis. The slurry was then filtered through Whatman No.1 filter paper and the filtrate analysed for sulfate, potassium, and iron using ICP-OES or AAS. The residues were characterised by XRD, XRF, ICP-OES, and AAS.

The alkaline decomposition-cyanidation experiments were done as previously but with NaCN additions from 1 to 10 g/L, added after reaching the desired pH so as to establish the behaviour of the ferric iron as a function of the cyanide concentration. The slurry was then filtered through Whatman No.1 filter paper and the filtrate analysed for sulfate, potassium, and iron using ICP-OES. The particle size distribution (volume based) of the decomposition product was done on the wet sample using six runs on a Malvern Mastersizer 2000.

The dissolution of the jarosite in the alkaline solution was also followed using the same procedure as before, but taking 10 ml samples collected at 10 minute intervals using a syringe and filtering the sample through Whatman No.1 paper. The experiments were done in duplicate to ensure reproducibility. The decomposition of the jarosite was monitored by analysing for potassium using ICP-OES. No correction was required for

the samples removed as a fraction of the homogeneous suspension was taken following the procedure suggested by Madden et al., (2012).

3.3.3 Alkaline decomposition with preconditioning and cyanidation

The alkaline decomposition of the jarosite with alkaline preconditioning was investigated by exposing it to an alkaline solution at 25ºC by suspending 7.0 g (~3.0 g dry basis) of wet jarosite in 500ml water with a pH of 10.5 to 11, adjusted using CaO, while stirring at 300 revolutions per minute. The jarosite/decomposition products (amorphous ferric hydroxide) containing solution was conditioned for periods ranging from 0 to 24 hours with stirring before adding 4.5g of NaCN, and then leached for another 24 hours. The slurry was then filtered through Whatman No.1 filter paper and the filtrate analysed for iron using ICP-OES.

3.3.4 Speciation of iron in solution

The speciation of the iron in solution was investigated using cyclic voltammetry to indicate the oxidation state of the iron present in solution. The cyclic voltammogram was recorded with a potentiostat using a conventional three electrode cell comprised of a graphite electrode, a graphite counter electrode (bagged in polyethylene), and an Ag/AgCl reference electrode, and at a temperature of 26°C. The potential was scanned from 0.5 to -0.2V(SCE) at a scan rate of 1mV/s, noting that the standard reversible potential for the $Fe(CN)_6^{3-}/Fe(CN)_6^{4-}$ half cell is 0.36V relative to the Ag/AgCl reference electrode. The $Fe(CN)_6^{3-}$ should be reduced to the $Fe(CN)_6^{4-}$ at potentials less than 0.36V and the $Fe(CN)_6^{4-}$ oxidised to $Fe(CN)_6^{3-}$ at potentials greater than 0.36V.

3.3.5 Dissolution in carboxylic acids

The possibility to remove the labile iron present in the jarosite by pre-leaching with carboxylic acids like oxalic, citric and tartaric acid was evaluated using the same leaching procedure as previously described but with the equivalent amount of acid, at a mole ratio of 1:4 for iron: carboxylic acid and monitoring the iron in solution.

3.4 Application to gold ore leach tests on BIOX® products

3.4.1 Ore sample preparation

The biooxidised gold ore residue cyanidation feed samples, respectively, oxidised with mesophile bacteria only and also with further thermophile oxidation, were received from Barberton Mine. Two sets of samples were received, one from a pilot plant and another from the main plant cyanidation feed. Samples from the pilot plant were received already dried and milled. The cyanidation feed samples were received in a wet state and air dried for two days, after which the lumps were ground using a mortar and pestle. The samples were mixed, coned and quartered and representative samples used in the test work. The particle size distribution was carried out using the wet screening method. The milled samples were further milled in a tungsten carbide vessel using a swing mill for analysis using XRD and XRF.

3.4.2 Leaching of the ore

The leaching of the gold biooxidation residues was done in the as received condition for the pilot plant samples and with the dried cyanidation feed samples using a pulp with a solids to liquid ratio of 40 mass percent, i.e. with 400g of the ore added to 1 litre of distilled water. The pH of the pulp was adjusted to 10 to 10.5 using CaO. 8g NaCN was then added which is equivalent to the 20 kg NaCN/ton of ore used in the Barberton plant. The mixture was stirred at 500 revolutions per minute for 24 hours with air bubbling. Following the leach the pulp was filtered through Whatman No.1 filter paper, and the filtrate analysed for the relevant metal ions by ICP-OES. The free cyanide was analysed by titration with $AgNO_3$ to the rhodanine end point. The residue was washed with distilled water and air dried for two days and milled for analysis using XRD and XRF.

Further experiments were done as above varying the amount of NaCN added from 2 to 20 kg NaCN/ton of ore, i.e. 0.8 to 8g NaCN added to the 400g sample of ore.

4 RESULTS AND DISCUSSION

4.1 Synthesis and reactivity of jarosite in alkaline media

4.1.1 Jarosite precipitation

Significant conversion of the iron to jarosite was achieved during the precipitation process as indicated by the mass balance in Table 4.1 and the XRD spectrum in Figure 4.2, with more than 86 mass percent conversion of the iron in solution achieved (calculations shown in Appendix 3). The terminal concentration of ferric iron in solution of 1.24 g/L (0.022M) indicates that equilibrium was not achieved as the calculated solubility is about three orders lower (5.25×10^{-5}M), using Gibbs free energy data from the NBS database (Stabcal W32 software) illustrated in Figure 4.1. The XRD pattern obtained for the precipitate indicated that it was an end-member potassium jarosite and that there was no indication of any other crystalline compound in the precipitate. The particle size distribution for the synthesised jarosite is shown in Figure 4.3 indicating a volume based P_{80} of 22 µm and a volume weighted mean of 19 µm.

Table 4.1. Iron (3+) precipitation as jarosite from an initial concentration of 9 g/L Fe^{3+} (0.161 M)

Runs	1	2	3	4	5	6	7	Average	Standard deviation
Residual Fe in solution (g/L)	1.19	1.23	1.24	1.29	1.25	1.24	1.25	1.24	0.03
Residual Fe mass percent	13.2	13.7	13.7	14.3	13.9	13.7	13.9	13.8	0.3
Precipitated Fe mass percent	86.8	86.3	86.3	85.7	86.1	86.3	86.1	86.2	0.3

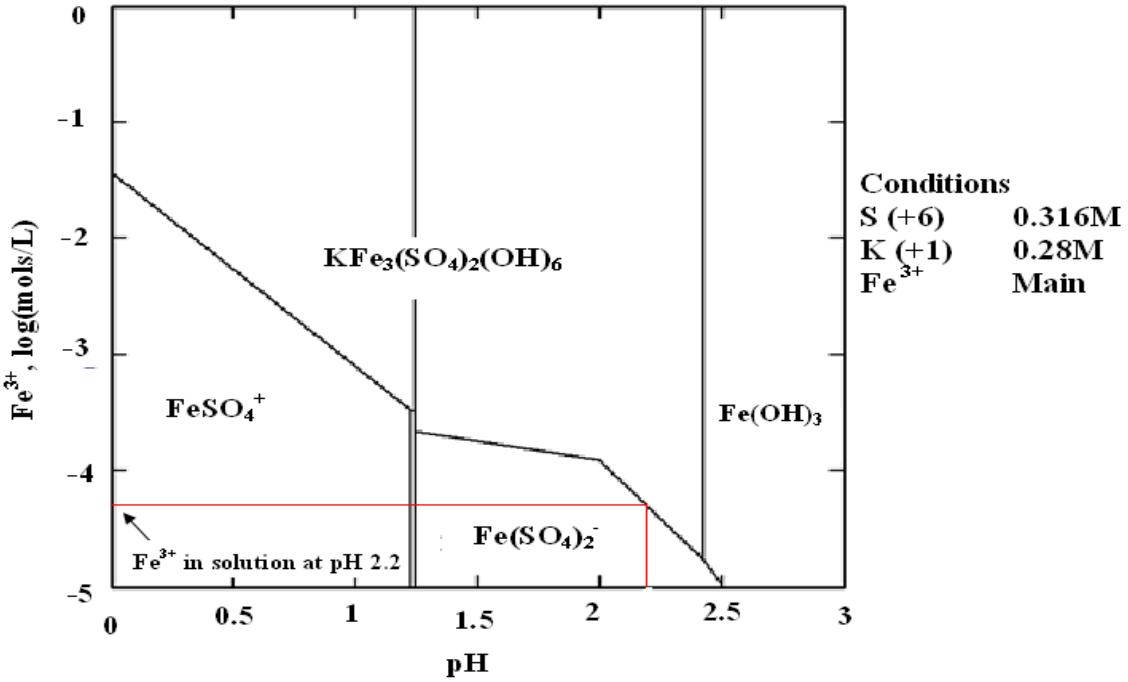

Figure 4.1. Solubility of Fe^{3+} as a function of the pH in the presence of SO_4^{2-} (0.316M) and K^+ (0.28M) at 45ºC (NBS data base, software: Stabcal W32, Gibbs free energy data in Appendix 4)

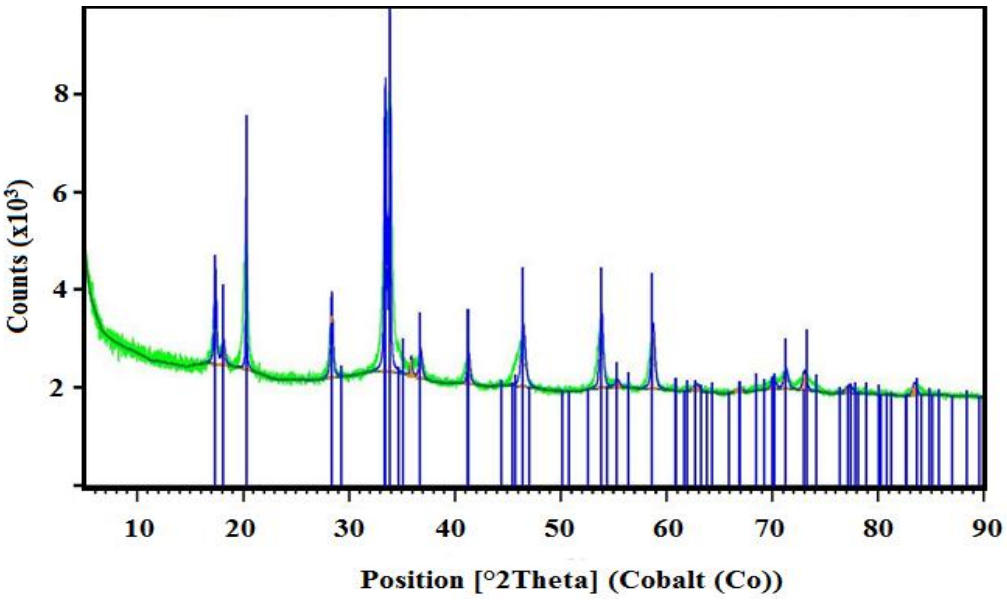

Figure 4.2. XRD pattern of the synthetic jarosite precipitate

The measured and stoichiometric chemical compositions are indicated in Table 4.2. The potassium content is lower than the expected value of 7.8 mass percent, and is probably due to substitution by the hydronium and/or ammonium ions also present in the solution.

Table 4.2. Analytical results for synthetic jarosite

Element	1	2	3	Average	Standard deviation	Ideal potassium jarosite
Iron (Fe) (mass percent)	30.0	29.8	29.9	29.9	0.1	33.5
Potassium (K) (mass percent)	7.5	7.3	7.2	7.3	0.2	7.8
Sulfur (S) (mass percent)	10.0	9.5	10.1	9.8	0.3	12.8
Phosphorous (P) (mass percent)	3.3	3.2	3.2	3.2	0.1	-

The precipitate also contained 3.2 mass percent phosphorous originating from the phosphate in the mineral formulation. No crystalline phosphates were detected by XRD indicating that the phosphate is probably present as an amorphous phase, or chemisorbed to particle surfaces, or occluded within the structure of the jarosite. Phosphate is often chemisorbed to the surfaces of iron and aluminium minerals, especially at low pH where surface functional groups tend to be positively charged, as has also been found by Bigham, et al., (2010). The composition of the jarosite formed is also consistent with the findings of Dutrizac and Chen (2010) who reported that as the concentration of phosphate in the synthesis solution increased the phosphate content in the precipitate increased and that these increases were linked to decreases in the sulfate content. They also found that the iron content decreased systematically as the phosphate concentration increases, but that the overall reduction in the iron content was minor and the potassium content remained essentially constant.

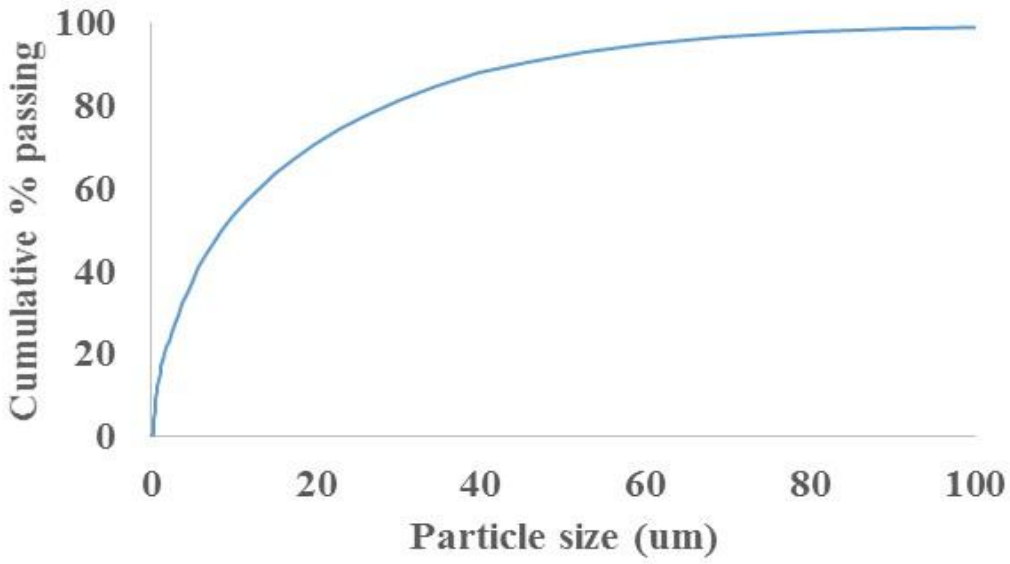

Figure 4.3. Size distribution of the synthetic jarosite (data in Appendix 5)

4.1.2 Jarosite alkaline decomposition and cyanidation

The jarosite was substantially converted to ferric hydroxide during exposure to the alkaline environment as indicated by the change in colour of the solids from yellow to reddish (Roca et al., 1993). In order to examine the mineralogical changes after decomposition the residue was again analysed by XRD and ICP-OES (after hydrochloric acid digestion). The XRD pattern of the decomposed product did not indicate the presence of any crystalline material indicating that the decomposition product is amorphous in nature as illustrated in Figure 4.4.

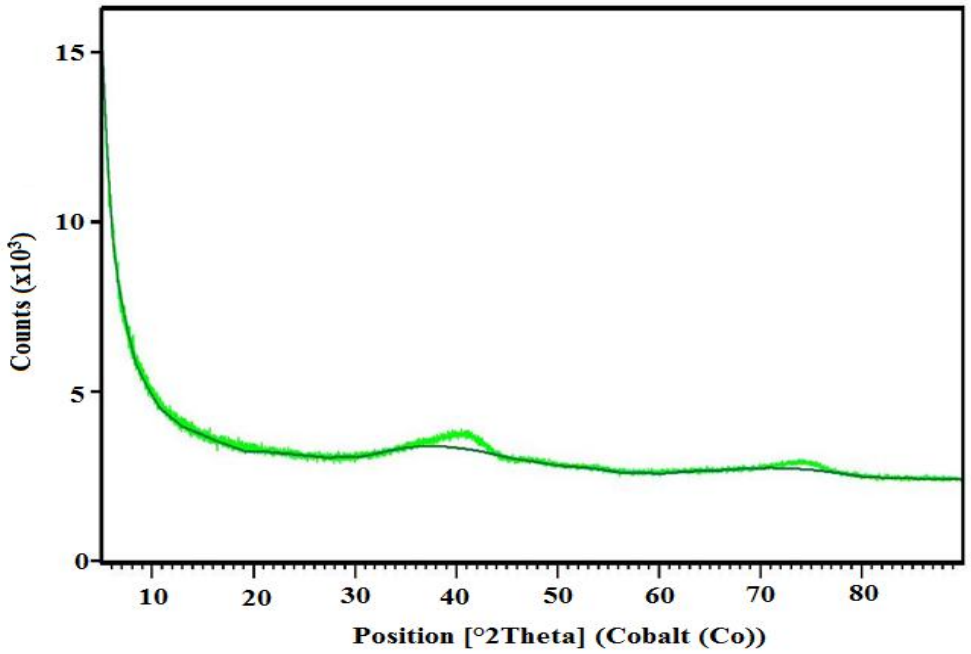

Figure 4.4. XRD pattern of the jarosite dissolution products in alkaline media

The particle size distribution for the decomposition product is shown in Figure 4.5 and indicates a volume based P_{80} of 24 µm and a volume weighted average mean of 14 µm. The AAS analysis of the residue showed that it contained 48.9 mass percent of iron, which is close to the stoichiometric content of iron in $Fe(OH)_3$, i.e. 52.3 mass percent (calculations shown in Appendix 3). The potassium and sulfate detected in solution indicate that these species were released during the decomposition of the jarosite. A mass balance based on the potassium and sulfate in solution indicated that about 99 mass percent of the jarosite decomposed in the alkaline solutions, with and without cyanide.

The decomposition of jarosite as a function of time, as indicated by the concentration of potassium in solution, increased with time with 70 mass percent decomposing in 100 minutes. The results were also interpreted in terms of the fractional conversion considering the jarosite particles to be spheres with the reaction rate controlled by either mass transfer to or away from the particle, diffusion through the product layer, or the reaction at the interface with the unreacted core as indicated in Appendix 7. These models were developed for particles of a single size and its application is not representative of the system due to the non-uniformity of the particle sizes. Integration over all particle sizes would be necessary, but was beyond the scope of this study.

However, the applicability of this approach, which was developed for single particles, to collections of differently sized particles was investigated by Chao and Sohn (2015). They characterized the effect of the size distribution in terms of the coefficient of variance (CV), which is the ratio of the standard deviation to the mean of the size distribution. They showed that the reaction kinetics deviates from that for a uniform particle size as the CV values increases and the particle shape deviates from spherical toward flat. They showed that the effect of the particle size distribution for Gate-Gaudin-Schuhmann (GGS) distribution on the kinetics is insignificant for CV values up to 0.5, and for Rosin-Rammler-Bennet (RRB) and Gamma distributions that the effect is tolerable up to the CV value of 0.75. The CV of the RRB distribution fit for the jarosite was calculated to be 0.15, and that for the GGS was 0.5 as indicated in Appendix 5. The CV for the GGS distribution is at the maximum acceptable level and that for the RRB distribution is low, which indicates that in the present case the shrinking core model may be used to interpret the kinetics of the conversion process without incurring significant error. Some idea of the rate controlling step in the decomposition of the jarosite may thus be gained by plotting the fractional conversion relationships based on shrinking core model as a function of time as proposed by Levenspiel (1999). These plots are shown in Figure 4.6 and indicate that the results are not well described by these relationships although some case may be made for a mechanism in which the diffusion through the product layer is the controlling step in the reaction sequence, as that with the best fit with a R^2 of 0.96. This is at variance with other studies which found that the conversion was under chemical reaction control (Roca, et al., 2006; Patino, et al., 2013). It is proposed that this might be due to differences in the particle size distribution of the materials evaluated. The particle size distributions of the jarosite and that of the decomposition product (amorphous $Fe(OH)_3$) are similar with volume weighted averages of 19 and 14 μm respectively and also as illustrated in Figures 4.3 and 4.5. This is in agreement with the shrinking core model in which it is presumed that the particle size does not change significantly as the reaction proceeds.

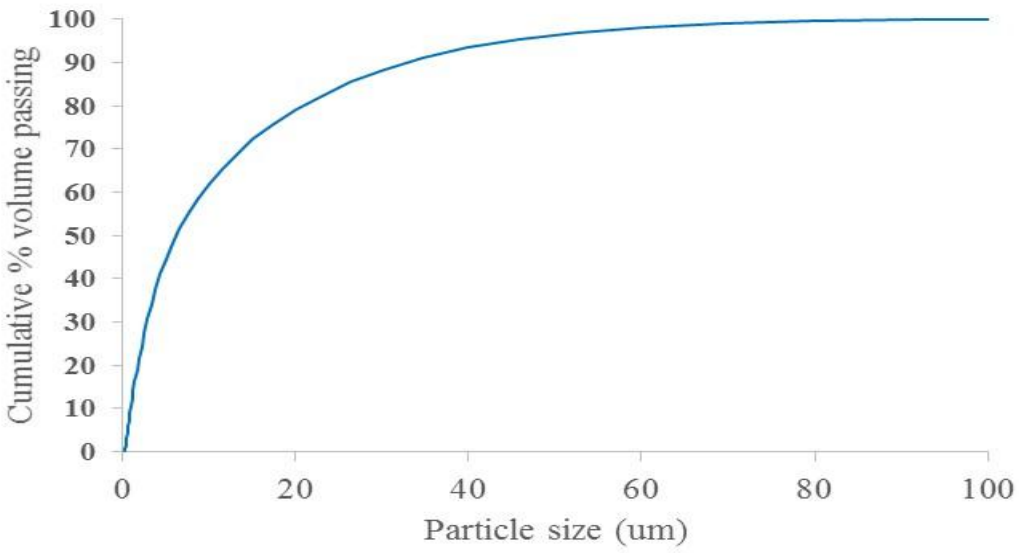

Figure 4.5. Particle size distribution of jarosite decomposition product (amorphous $Fe(OH)_3$) (data in appendix 6)

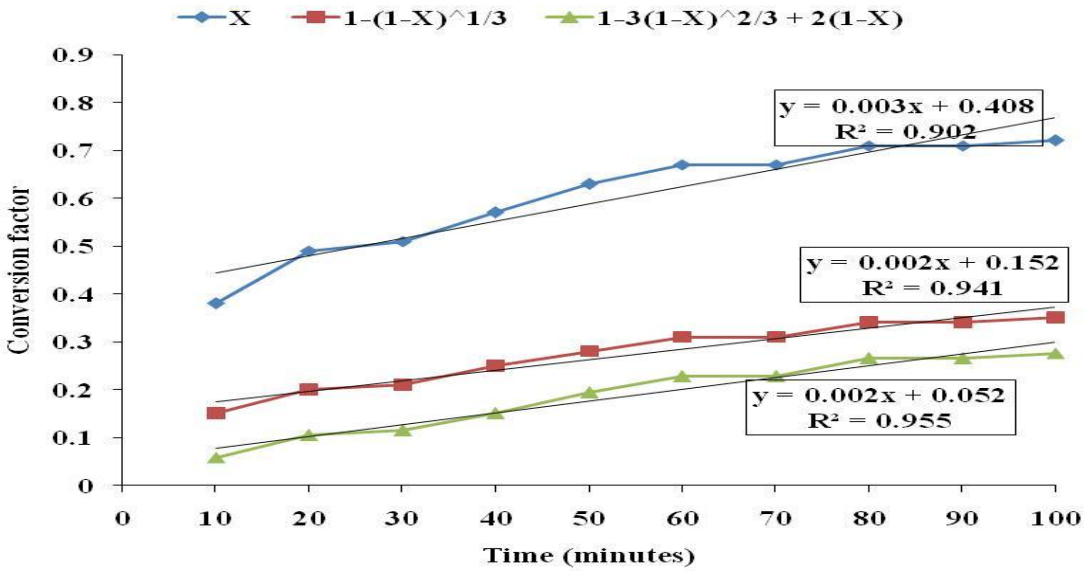

Figure 4.6. Fractional conversion of the precipitated potassium jarosite in an aqueous solution at pH 11, 26ºC and stirred at 300 revolutions per minute following the potassium concentration in solution. Conversion relationships for sphere with ash layer or shrinking sphere particles with various rate controlling steps and linear fits of the data also indicated (data in Appendix 7)

4.1.3 Alkaline decomposition with and without preconditioning followed by cyanidation

The results reported above indicated that the laboratory prepared jarosite substantially decomposed to a ferric hydroxide precipitate during exposure to alkaline conditions. Leaching in aqueous cyanide indicated that this ferric hydroxide is labile in the presence of cyanide, with leaching increasing with cyanide concentration as illustrated in Figure 4.7. The iron probably dissolved as the hexacyanoferrate(III) complex ($Fe(CN)_6^{3-}$) which is thermodynamically stable under these conditions, as shown in Figure 1.2. The iron is probably also reacting with the cyanide during the transformation of the jarosite, i.e. before precipitation as ferric hydroxide, as the cyanide ion would form the thermodynamically more stable species.

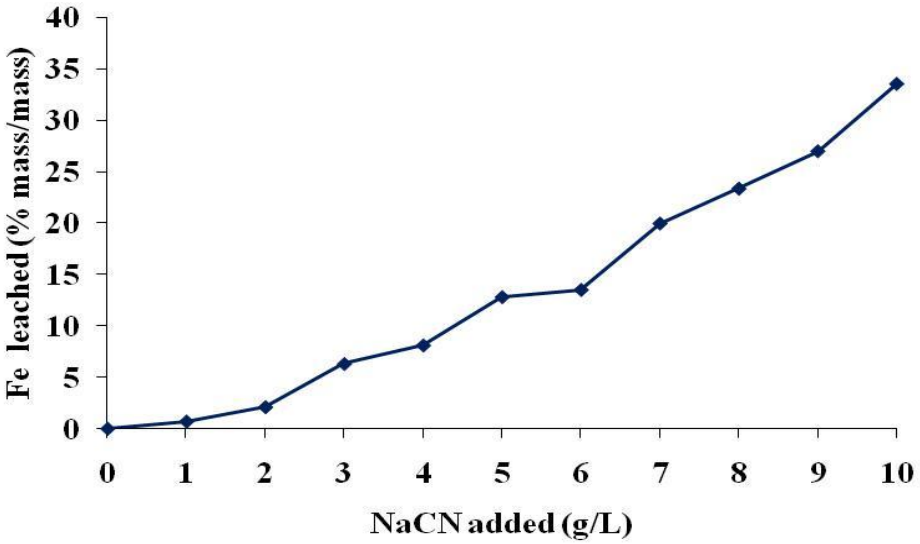

Figure 4.7. Leaching of iron from jarosite decomposition product in alkaline cyanide solution at pH 10.5 - 11, 25°C for 24 hours as a function of cyanide in solution (data in Appendix 8)

The stabilisation of the iron hydroxide precipitate by preconditioning was investigated by conditioning the jarosite in the alkaline solution for periods ranging from 3 to 24 hours to allow time for its conversion to ferric hydroxide and the precipitate to coagulate and form a stable crystalline precipitate before adding the cyanide to the solution. It was indeed found that pre-conditioning of the jarosite decomposition

products (amorphous ferric hydroxide) reduced leaching of ferric ions in the aqueous cyanide solution. The results are shown in Appendix 9. The decrease was more pronounced after three hours of alkaline pre-conditioning; thereafter the decrease was small as shown in Figure 4.8.

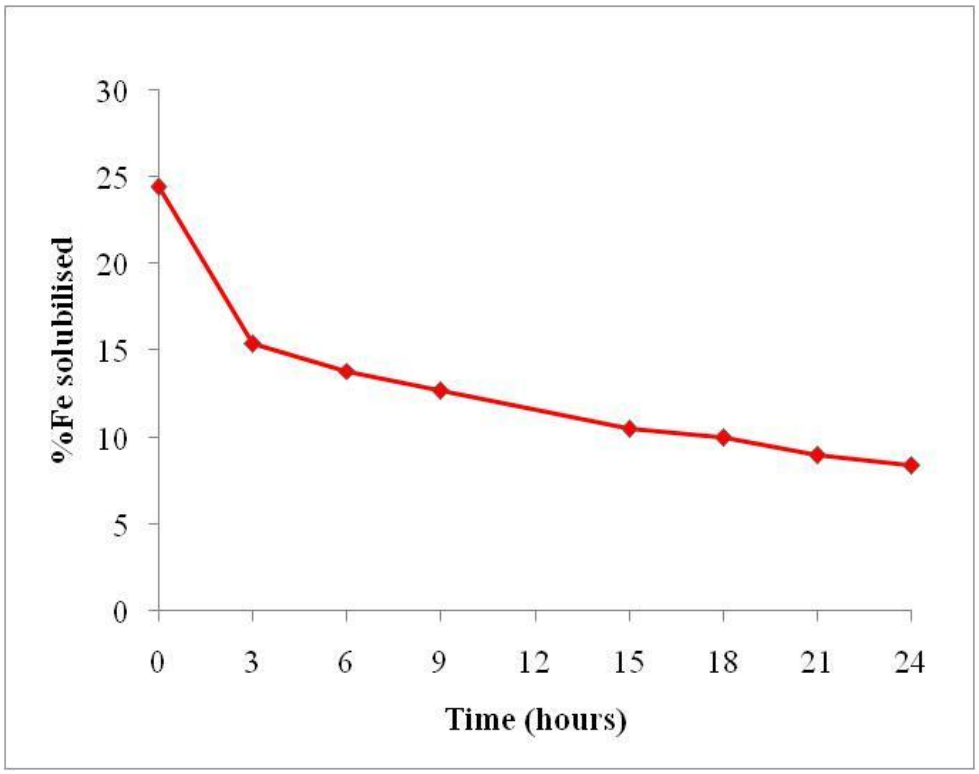

Figure 4.8. Leaching of iron from jarosite decomposition product in alkaline aqueous cyanide solution after alkaline preconditioning at pH 10.5 - 11, 25°C and 8g/l NaCN (data in Appendix 9)

4.1.4 Speciation of iron in solution

The polarization behaviour of the iron cyanide species formed on a graphite electrode was determined to give some indication of the oxidation state and reversible potential of the half cell. The voltammogram for the alkaline cyanide leach solution for 4g NaCN and 3g jarosite per litre of water was measured in the range 0.5V to -0.2V (relative to silver/silver chloride) is shown in Figure 4.9. The scan from 0.5 to -0.2V indicates that $Fe(CN)_6^{3-}$ is probably reduced to $Fe(CN)_6^{4-}$ and that on the reverse scan $Fe(CN)_6^{4-}$ is oxidised to $Fe(CN)_6^{3-}$ when considering the standard reversible potential for this halfcell. The voltammogram also indicates that iron existed in the +3 oxidation state as there is no oxidation peak at ~0.28V shown on the initial negative scan in Figure 4.9.

The speciation of iron in solution was also confirmed by the qualitative colour change test of the solution to blue when ferrous iron is added to the solution resulting in the formation of Prussian blue ($KFe^{III}Fe^{II}(CN_6)$) (Vogel, 1979).

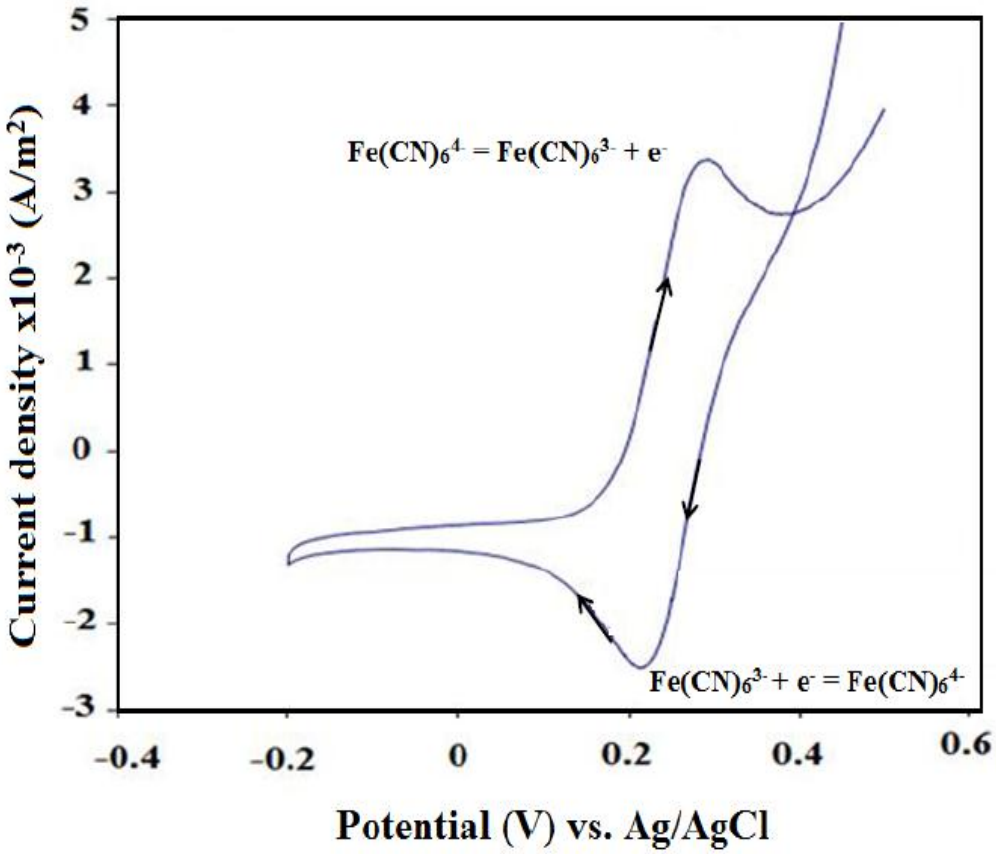

Figure 4.9. Cyclic voltammogram obtained on a graphite electrode for the leach solution, scan rate 1 mV/s, and scan range 0.5 to -0.2V vs. Ag/AgCl

4.1.5 Dissolution of jarosite in carboxylic acids

The dissolution of the jarosite in organic acids as a means to remove the jarosite from the solids was evaluated using a stirred batch reactor at 25°C. All the jarosite dissolved in aqueous solutions of oxalic acid, but only 29 mass percent in citric acid, and 10 mass percent in tartaric acid as shown in Figure 4.10. Other metal cations present in the residue will probably also be solubilised by complexing with the oxalate. The removal of ferric precipitates should also result in the exposure of more gold to cyanide since the ferric precipitates may occlude some of the gold.

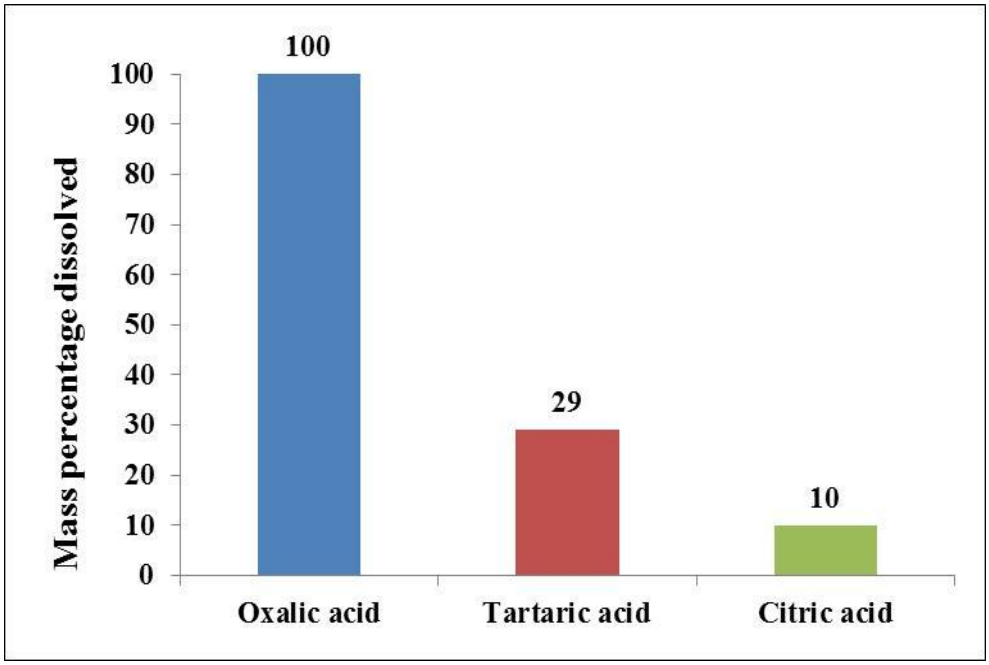

Figure 4.10. Dissolution of jarosite in aqueous organic acids after 6 hours at 25°C (data in Appendix 10)

The pretreatment of the jarosite with carboxylic acids will, however, pose challenges. In addition to the additional cost of the acid, the residual carboxylic acids may foul the activated carbon used for the recovery of the gold and reduce its capacity. Thus the organic acids will have to be removed or an alternative option for the recovery of the gold like solvent extraction or ion exchange should be used. This will most probably make the use of organic acids to remove the iron containing precipitates unattractive.

4.2 Application to gold ore – leach tests on BIOX® products from Barberton Mine

4.2.1 Analysis of the pilot plant BIOX® products

The sieve test results given in Table 4.3 showed that, respectively, 97 mass percent of the mesophile and 99 mass percent of the thermophile products passed the 75µm screen. This rather fine particle size is in part due to the reduction of the particle size that results from the bioleaching process.

Table 4.3. Sieve analyses results for the pilot plant mesophile and thermophile biooxidation product samples as received from the mine (calculations shown in Appendices 11 and 12)

	Pilot plant mesophile BIOX® product	**Pilot plant thermophile BIOX® product**
Sieve size (µm)	Mass percent passing	Mass percent passing
212	100	100
150	99	100
75	97	99
53	95	98

The characterisation of the mineralogical composition of the biooxidation product samples was performed by XRD analysis and the relative phase amounts (mass percent) were estimated using the Rietveld method (Autoquan Program). The results are shown in Table 4.4 and the XRD patterns are given in Appendices 13 and 14.

The XRD analysis of the mesophile and thermophile biooxidation product samples did not show the presence of residual pyrite and arsenopyrite minerals (some probably still present but below the detection limit) indicating high conversions of the sulfide minerals. However, the XRD analyses indicated the presence of iron containing minerals such as potassium jarosite ($KFe_3(SO_4)_2(OH)_6$), at 7 mass percent in the mesophile product, and 15 mass percent in the thermophile product, as well as 11 mass percent scorodite ($FeAsO_4 \cdot 2H_2O$) in the thermophile product. These results indicate that the formation of crystalline iron precipitates is as expected favoured by the higher temperature of the thermophile process. The other minerals recognized in the biooxidation products were gypsum ($CaSO_4.2H_2O$), quartz (SiO_2), talc

($Mg_3Si_4O_{10}(OH)_2$), muscovite ($KAl_2(AlSiO_3O_{10})(F,OH)_2$), hornblende ($Ca_2(Mg,Fe)_4Al(Si_7Al)O_{22}(OH,F)_2$), and chlorite $(Fe,Mg,Al)_6(Si,Al)_4O_{10}(OH)_8$).

Table 4.4. Semi-quantitative XRD results for the pilot plant mesophile and thermophile biooxidation product samples as received from the mine (calculations shown in Appendices 15 and 16)

	Pilot plant mesophile BIOX® product		**Pilot plant thermophile BIOX® product**	
Mineral	Mass percent	Standard deviation	Mass percent	Standard deviation
Jarosite	7	1	14.8	0.4
Gypsum	26.8	0.1	47	1
Scorodite			10.6	0.9
Chlorite	4	1	1.7	0.2
Hornblende	4	1	1.4	0.6
Muscovite	18	2	6	3
Quartz	30	1	15.2	0.7
Talc	10	2	3.5	0.3

The XRF analytical results in Tables 4.5 and 4.6 indicate higher iron and sulfur contents in the thermophile than in the mesophile biooxidation product which is consistent with the higher contents of jarosite and gypsum detected by XRD.

The thermophile biooxidation product contains high arsenic (4.4 mass percent) and the mesophile biooxidation product contains low arsenic (0.3 mass percent); the arsenic was detected as scorodite by XRD.

Table 4.5. XRF results for the pilot plant mesophile biooxidation product and cyanide leach residue (calculations shown in Appendices 19 and 20)

	Pilot plant mesophile BIOX® product		Cyanide leach residue	
Analyte	Mass percent	Standard deviation	Mass percent	Standard deviation
S	6.1	0.2	4.68	0.04
Ca	6.6	0.2	6.8	0.1
Fe	4.1	0.2	3.4	0.2
Mg	2.82	0.03	2.48	0.03
K	2.70	0.03	2.9	0.1
As	0.31	0.01	0.23	0.03
Ni	0.052	0.004	0.0157	0.0001
Mn	0.037	0.001	0.0264	0.0003
Cu	0.0347	0.0005	0.027	0.001
Au	0.0125	0.0006	<0.01	
Zn	0.0087	0.0005	<0.01	
Co	0.0074	0.0003	<0.01	
Si	22.6	0.4	24.8	0.2

Table 4.6. XRF results for the pilot plant thermophile biooxidation product and cyanide leach residue (calculations shown in Appendices 21 and 22)

	Pilot plant thermophile BIOX® product		Cyanide leach residue	
Analyte	Mass percent	Standard deviation	Mass percent	Standard deviation
S	9.2	0.1	8.7	0.5
Ca	12	1	13.1	0.6
Fe	10.9	0.9	9.9	0.9
Mg	0.94	0.02	0.88	0.06
K	1.8	0.1	1.7	0.1
As	4.4	0.2	4.3	0.1
Ni	0.006	0.002	<0.01	
Mn	0.008	0.001	0.0070	0.0004
Cu	0.011	0.001	0.0081	0.0003
Au	<0.01		<0.01	
Zn	0.0048	0.0002	<0.01	
Co	0.006	0.002	<0.01	
Si	12.2	0.5	13.0	0.4

4.2.2 Leaching of the pilot plant BIOX® products

The leach solutions obtained after the alkaline cyanide leach were analysed by ICP-OES for the relevant ions with the results shown in Table 4.7. The concentration of sulfur was significantly higher in the mesophile compared to the thermophile leach solution. The sulfur in the leach solutions may be attributed to the release of sulfate during the decomposition of jarosite and the labile sulfur compounds which are present in the residues that may react with cyanide to form thiocyanate. In the thermophile residue most of the labile sulfur compounds have been oxidised to sulfate, that were not carried over with the residue or formed insoluble compounds that did not leach in the aqueous alkaline cyanide solution. Iron was detected in the leach solutions contributing, respectively, 11 and 19 mass percent of the cyanide consumption for the mesophile and thermophile products as illustrated in Figure 4.11 and Appendix 23. The iron is probably coming from the decomposition of jarosite and the increase in iron in the

thermophile leach solution is consistent with its higher jarosite content. In practice only 5 to 8 kg NaCN/t of ore is added during the cyanidation of thermophile biooxidation product and the contribution of iron to cyanide consumption would thus be a more significant portion of the total cyanide consumption.

The concentration of potassium in the leach solutions is unexpectedly low, based on the leaching of potassium jarosite, which may indicate that a mixture of jarosites is present in the biooxidised products with the decomposition of other types of jarosites e.g. ammonium and hydronium jarosites, contributing to cyanide consumption.

The concentrations of Cu, Au, Zn, Ni, Ag, Co, and Mn ions in the thermophile leach solution were observed to be lower than those in the mesophile leach solution which may be due to the removal by dissolution of the parent minerals during the thermophile process. The scorodite seems to be very stable as no arsenic was detected in the leach solution which ties in with only a slight decrease in the scorodite in the solid residues.

The relatively low concentration of gold in the thermophile leach solution was unexpected but also indicative of the difficulty to obtain representative samples from operating plants.

The contribution of metal cyanide complexes to cyanide consumption was not very significant with 1.4 and 0.5 mass percent of the cyanide consumption for the mesophile and the thermophile products leach respectively.

Table 4.7. Chemical compositions of leach solutions obtained after 24 hours of alkaline cyanide leaching of the pilot plant mesophile and thermophile biooxidation products

Analyte	Mesophile	Thermophile
	mg/L	mg/L
Fe	173	291
K	2	5
Total S	1890	1002
Cu	8	5
Zn	3	1
Ni	19	6
Au	52	11
Ag	2	0.3
Co	2	0.3
Mn	3	1

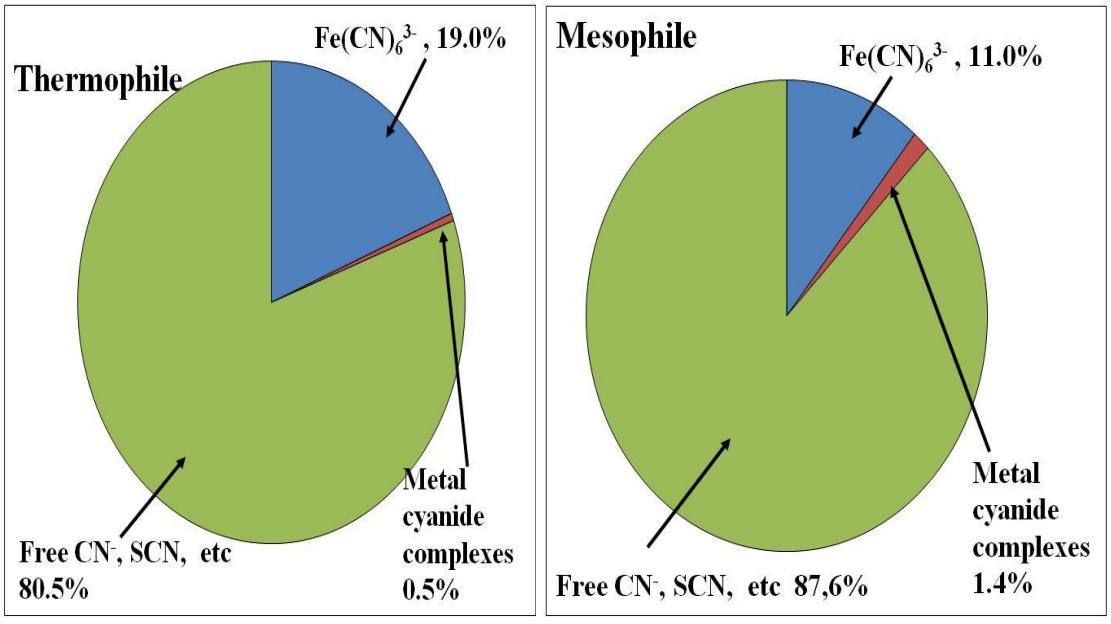

Figure 4.11. Cyanide in solution distributions at the end of the pilot plant (BIOX®) mesophile and thermophile samples leach tests (data in Appendices 23, 24, and 25)

However, the dissolution of the process jarosites was significantly lower than that of the synthetic jarosite after 24 hours exposure to cyanidation, as illustrated in Figure 4.12. For the mesophile BIOX® product 17 mass percent of the jarosites was converted to ferric hydroxide with only about half, i.e. 8 mass percent based on the original mass, dissolving as ferric cyanide. The conversions were slightly lower for the thermophile BIOX® product with 14 mass percent converted, and only 6 mass percent dissolving as ferric cyanide. These results are in line with the finding that the decomposition of natural jarosites is several orders of magnitude slower than that of synthetic jarosites in dilute aqueous solutions, with the presence of various ions in the pulp significantly affecting the dissolution of jarosites (Pritchettet al., 2012). The XRD analytical results of the cyanidation residues are shown in appendices 17 and 18.

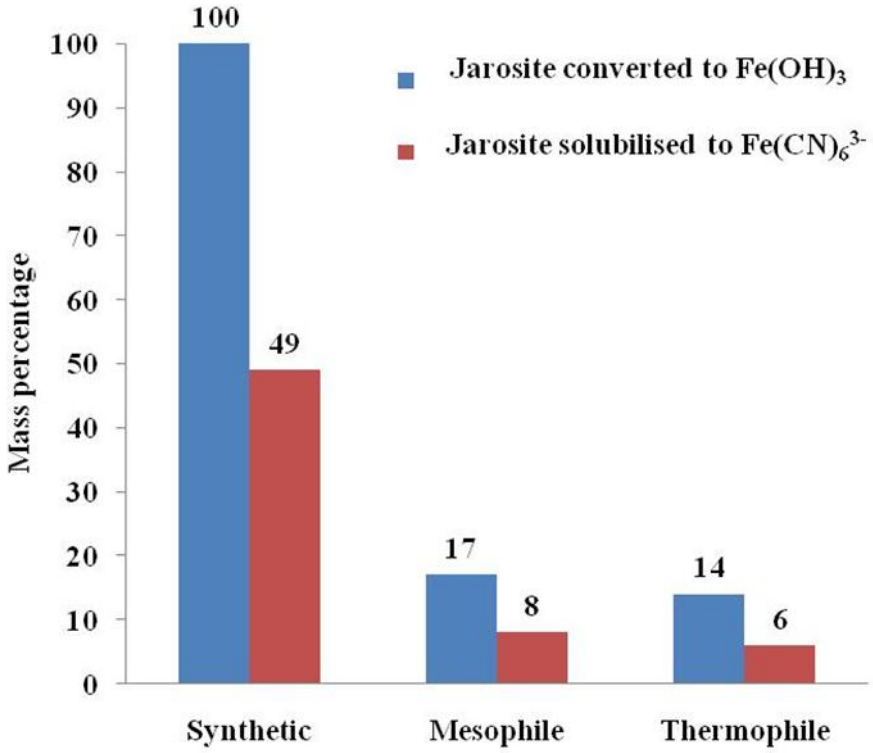

Figure 4.12. Comparison of jarosite converted and dissolved during a 24 hour leach of the synthetic and process jarosites with 9 g/L NaCN dosed (data in Appendix 26)

4.2.3 Leaching of iron and gold from the main plant BIOX® residues in aqueous alkaline cyanide solution

The leaching of iron and gold from the main plant BIOX® process cyanidation feed samples under gold leaching conditions with varying cyanide additions was investigated. The mineralogical and chemical analysis results of the main plant BIOX® residue samples are shown in Appendices 27 – 30. It was found that the iron in solution increased with added cyanide for both samples as illustrated in Figure 4.13. This is consistent with the earlier finding that the leaching of iron from jarosite decomposition products (amorphous ferric hydroxide) increases with cyanide concentration probably due to its effect on the reaction rate. Thus high cyanide additions promote iron leaching and its contribution to cyanide consumption.

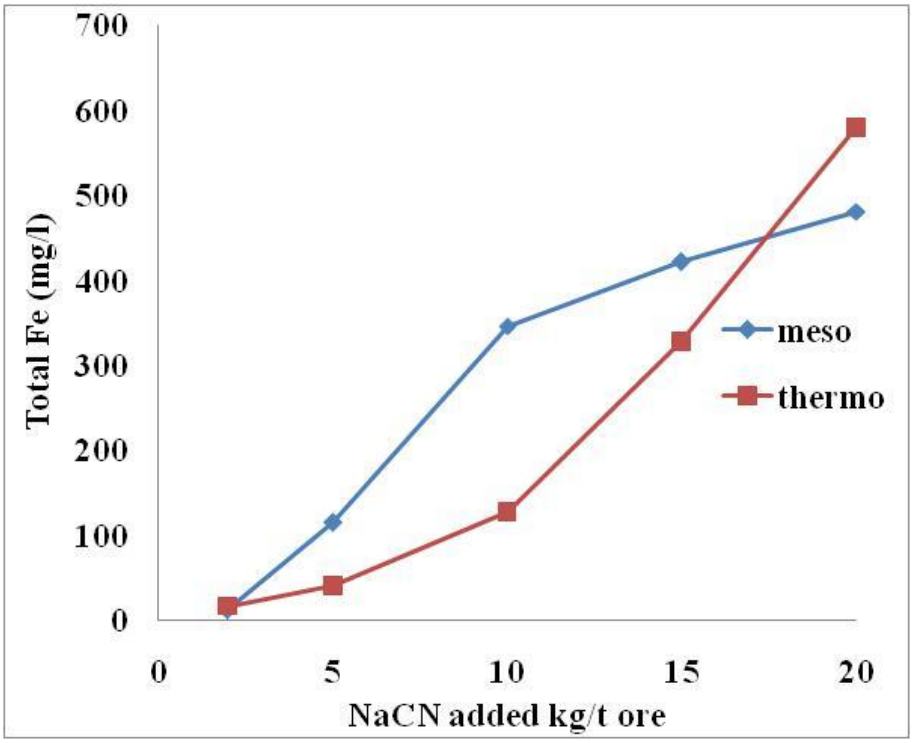

Figure 4.13. Iron leaching after 24 hours from mesophile and thermophile main plant BIOX® residues at pH 10.5 and 25°C (data in Appendix 31)

The concentration of total sulfur species in solution increased significantly with cyanide concentration as shown in Figure 4.14. The leaching of ferric hydroxide by cyanide affects the conversion of jarosite to ferric hydroxide, so at higher cyanide concentrations an increase in jarosite conversion is expected which results in the release of sulfate into solution, hence an increase of total sulfur species in solution with cyanide concentration

is expected. It can also be assumed that the increase in cyanide concentration also increases the kinetics of the reaction of reduced sulfur species with cyanide to form thiocyanate resulting in an increase in total sulfur in solution.

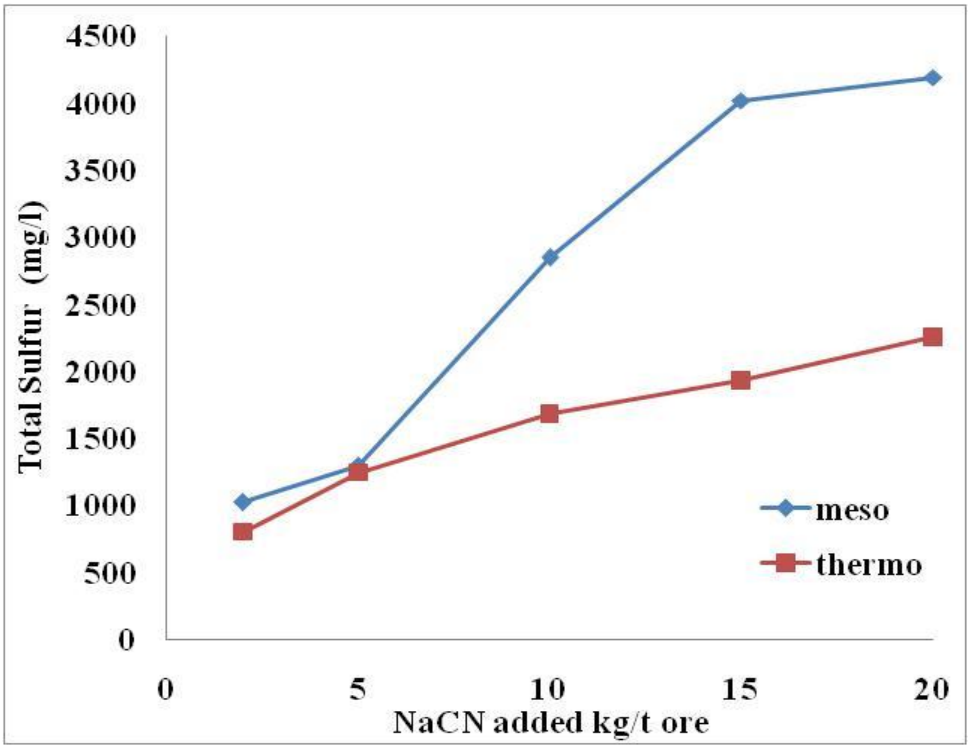

Figure 4.14. Total sulfur leached as a function of added cyanide after 24 hours from mesophile and thermophile main plant BIOX® residues at pH 10.5 and 25°C (data in Appendix 32)

The concentration of gold in the leach solution for the thermophile residue increased significantly up to 5 kg NaCN per ton of ore but then remained relatively constant in the range of 5 to 20 kg NaCN/t ore, as illustrated in Figure 4.15. The high cyanide additions in this case thus only served to enhance the leaching of iron from jarosite decomposition products and to promote the reaction of reduced sulfur species with cyanide resulting in high cyanide consumption. From these results it can be concluded that the gold can be leached effectively from the thermophile residue at a NaCN dosage of 5 kg/t ore. However, in the case of the mesophile residue cyanidation the gold leached increased up to 20 kg NaCN per ton of ore added indicating that there is competition for the cyanide by other species present in the leach.

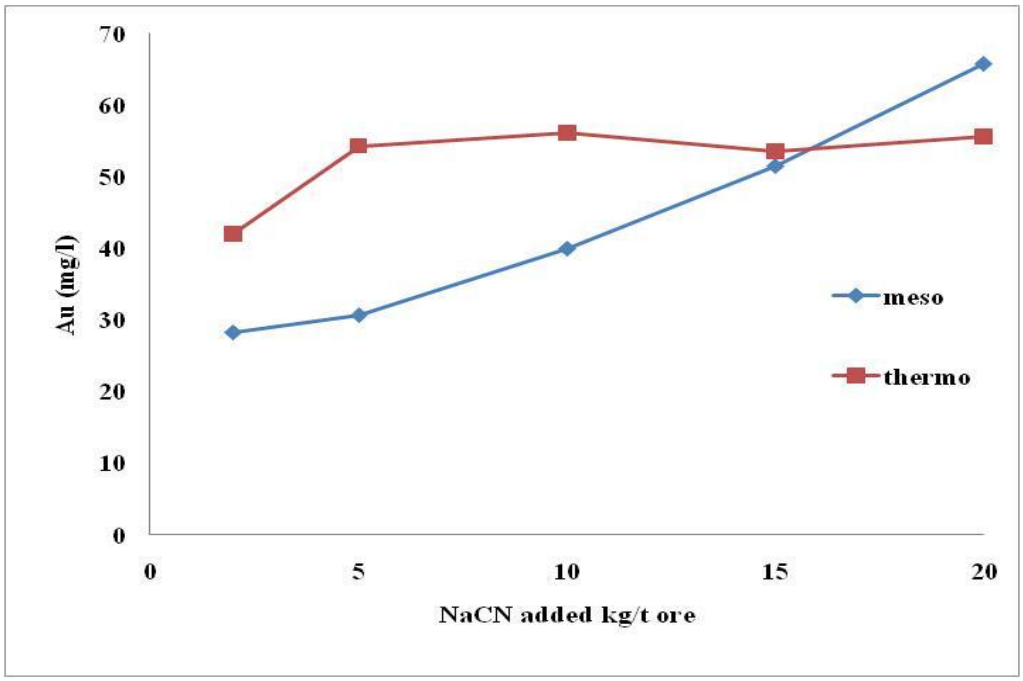

Figure 4.15. Gold leached as a function of cyanide added after 24 hours from main plant BIOX® mesophile and thermophile residues at pH 10.5 and 25°C (data in Appendix 33)

There was no detectable titratable free cyanide in the mesophile leach solutions at the end of the leaches illustrating the high demand for cyanide for this product. In case of the thermophile leach solutions the titratable free cyanide was observed to increase with cyanide addition as illustrated in Figure 4.16.

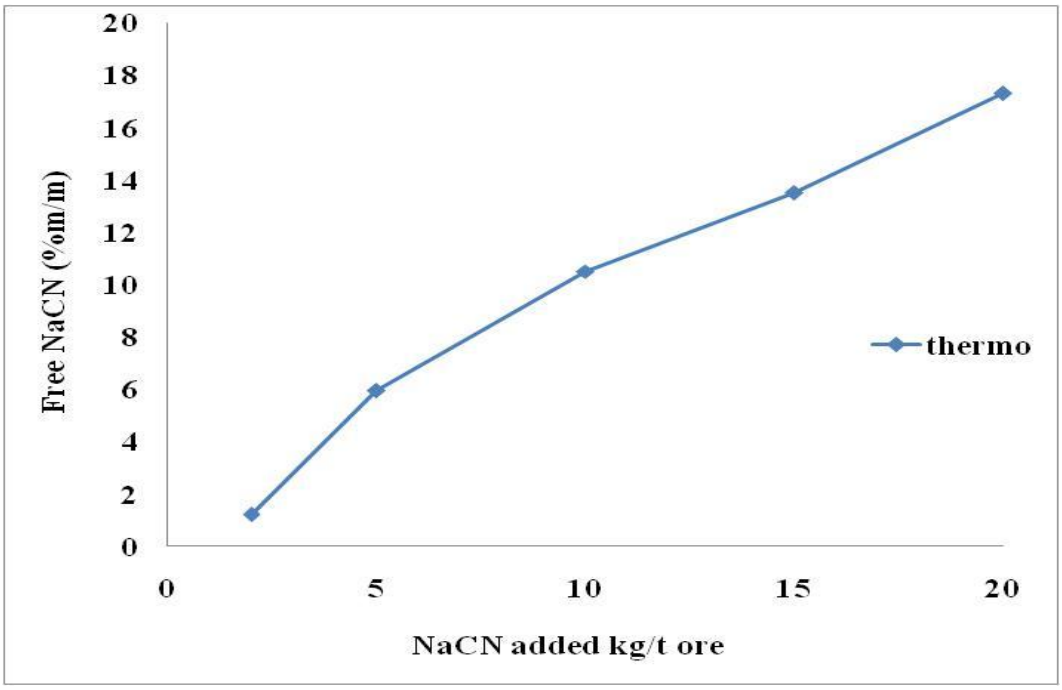

Figure 4.16. Free NaCN in solution as a function of cyanide added after 24 hours leaching of thermophile main plant BIOX® product from the main plant at pH 10.5 and 25°C (data in Appendix 34)

5 CONCLUSIONS AND RECOMMENDATIONS

The results of this study indicate that the formation of jarosite is possible under typical mesophile biooxidation conditions, i.e. in an aqueous sulfate solution containing potassium and ferric ions at pH 2.2 and a temperature of 45ºC. The produced jarosite was transformed to an amorphous ferric hydroxide, with the release of potassium and sulfate to the solution, when exposed to alkaline conditions typical of gold leaching with cyanide, i.e. pH 10.5 to 11 at 25°C. The kinetics of the conversion probably followed a shrinking core model with the diffusion through the product layer as the rate controlling step. The transformed jarosite (amorphous $Fe(OH)_3$) readily reacted with aqueous cyanide in alkaline media with the cyanide consumption favoured at higher cyanide concentrations for the 1 to 10 g/L cyanide concentration investigated. The consumption of cyanide by jarosite could thus be significant, but would obviously depend on how much jarosite is formed during the bioleaching process. Aging of the transformed jarosite (amorphous $Fe(OH)_3$) reduced its reactivity towards cyanide.

The removal of the iron from the solids by leaching with organic acids was investigated and it was found that the transformed jarosite readily leached in aqueous oxalic acid but only partially in citric and tartaric acids. However, the use of an oxalic acid preleach would apart from the cost implications not be attractive as the organic acid would probably also adsorb on the activated carbon used downstream for the recovery of the gold from the leached pulp, to reduce the rate of gold recovery.

The BIOX® products from Barberton mine were found to contain significant amounts of jarosites which indeed leached to form ferric cyanide during alkaline cyanidation, thus contributing to cyanide consumption. The leaching of iron from the BIOX® residues increased with the amount of jarosite present in the ore and also with an increase in the cyanide concentration, which promoted the leaching of ferric iron as the cyanide complex. The process jarosites were relatively more stable compared to the synthetic jarosites during the alkaline cyanidation process with a significantly slower dissolution rate, with only half of the jarosite converted to ferric hydroxide leached as ferric cyanide at the cyanide concentrations typical of gold leaching for BIOX® residues. The fresh BIOX® residues from the plant were observed to be more reactive than the matured samples from the pilot plant.

It may thus be concluded from the present work that the formation of jarosite is likely during the biooxidation of sulfide containing gold ores and with this tendency increasing for the higher temperature thermophile biooxidation. This may potentially increase the cyanide consumption during the subsequent alkaline cyanidation of the residue for the recovery of the gold as the iron containing solids will be carried forward to this leach where it would not be thermodynamically stable. The jarosites formed are, however, relatively stable and less than 10 mass percent leached under typical cyanidation conditions. However, although the jarosites may be expected to contribute to increased cyanide consumption during gold leaching, the cyanide consumption of the jarosites would typically be small compared to that of the labile sulfur species. The operation of the bioleaching at more acidic conditions, which should decrease the formation of the jarosites, could be considered but should be evaluated in the context of a possible decrease in the activity of the bioorganisms and the relatively small contribution of the jarosites to cyanide consumption.

6 REFERENCES

Akcil, A. and Deveci, H. (2010). Mineral biotechnology of sulfides. In Sudhir, K, Khan, A.A. and Rai, M.K. Geomicrobiology. Enfield, New Hampshire: Science Publishers.

Amankwah, R., Yen, W. and Ramsay, J. (2005). A two stage bacterial pretreatment process for double refractory gold ores. Minerals Engineering, 18, 103–108.

Babcan, J. (1971). Synthesis of Jarosite, $KFe_3(SO_4)_3(OH)_6$. Geol. Zb, 22(2), 299-304.

Bigham, J., Schwertmann, U., Traina, S., Winland, R. and Wolf, M. (1996). Schwertmannite and the chemical modelling of iron in acid sulfate waters. Geochimica et Cosmochimica Acta, 60(12), 2111-2121.

Bigham, J., Bhatti, T., Vuorinen, A., and Tuovinen, O. (2001). Dissolution and structural alteration of phlogopite mediated by proton attack and bacterial oxidation of ferrous iron. Hydrometallurgy, 59, 301-309.

Bigham, J., Jones, F., Ozkaya, B., Sahinkaya, E., Puhakka, J. and Tuovinen, O. (2010). Characterization of jarosites produced by chemical synthesis over a temperature gradient from 2 to 40ºC. International Journal of Mineral Processing, 94, 121-128.

Biomin. (n.d.). BIOX Technology. Retrieved on 09/08/2015, from http://www.biomin.co.za/biox/technology.html

Bosecker, K. (1997). Bioleaching: metal solubilisation by microorganisms. FEMS Microbiology Reviews, 20, 591-604.

Brierley, C. and Briggs, A. (2002). Selection and sizing of biooxidation equipment and circuits. (A. Mular, D. Halbe, and D. Baret, Eds.). Mineral processing plant design, practice and control. Society of Mining, Metallurgy and Exploration, 1540-1568.

Ciftci, H. and Akcil, A. (2010). Effect of biooxidation conditions on cyanide consumption and gold recovery from a refractory gold concentrate. Hydrometallurgy, 142-149.

Chao, J and Sohn H.Y. (2015). Effects of particle shape and size distribution on the overall fluid-solid reaction rates of particle assemblages. The Canadian Journal of Chemical Engineering, accepted article.

d'Hugues, P., Ceza, P., Cabral, T., Battaglia, F., Truong-Meyer, X. and Morin, D. (1997). Bioleaching of a cobaltiferrous pyrite: A continuous laboratory-scale study at high solids concentration. Minerals Engineering, 10(5), 507 – 527.

Deveci, H., Akcil, A. and Alp, I. (2003). Parameters for control and optimisation of bioleaching of sulfide minerals. Materials Science and Technology 2003 Symposium: Process Control and Optimization in Ferrous and Non Ferrous Industry, pp. 77-90.

Devici, H. (2002). Effect of solids on viability of acidophilic bacteria. Minerals Engineering, 15, 1181-1189.

Dew, D., Lawson, E. and Broadhurst, J. (1997). The BIOX process for biooxidation of gold bearing ores or concentrates. In D. Rawlings, Biomining: Theory, Microbes and Industrial Processes (pp. 45-79). Berlin: Springer.

Dousma, J. and de Bruyn P.L.? (1978). Hydrolysis-precipitation studies of iron solutions II. Ageing studies and the model for precipitation from Fe(III) nitrate solutions. Journal of Colloid and Interface Science, 64 (1), 154-170.

Dutrizac, J.E. (1983a). Factors affecting alkali jarosite precipitation. Metallurgical Transactions B, 14B, 531-539.

Dutrizac, J.E. (1983b). Jarosite-type compounds and their application. (K. O. Miller, Ed.) Hydrometallurgy: Research, Development and Plant Practice, 531-551.

Dutrizac, J.E. (1984). The behaviour of impurities during jarosite precipitation. (R. Bautista, Ed.) Hydrometallurgical Process Fundamentals, 125-169.

Dutrizac, J.E. (2008). Factors affecting the precipitation of potassium jarosite in sulfate and chloride media. Metallurgical and Materials Transactions B, 39(6), 771-783.

Dutrizac, J. and Chen, T. (2010).The behaviour of phosphate during jarosite precipitation. Hydrometallurgy, 102, 55-65.

Gramp, J., Jones, F., Bigham, J. and Touvinen, O. (2008). Monovalent cation concentrations determine the types of Fe(III) hydroxysulfates precipitates formed in bioleach solutions. Hydrometallurgy, 94, 29-33.

Jansen, A. and Webb, C. (1995). Ferrous sulfate oxidation using Acidithiobacillus ferrooxidans: A Review. Process Biochemistry, 30(3), 225–236.

Jin-yan, L., Xiu-xiang, T. and Pei, C. (2009).Study of formation of jarosite mediated by Acidithiobacillus ferrooxidans in 9K medium. Procedia Earth and Planetary Science, 1, 706-712.

Jones, F.S., J.M., Bigham, J.M., Gramp, J.P. and Tuovinen, O.H. (2014). Synthesis and properties of ternary (K-NH_4-H_3O) jarosites precipitated from Acidithiobacillus ferrooxidans cultures in simulated bioleaching solutions. Material Science and Engineering C, 44, 391-399.

Jones, L. and Hackl, R. (1999). Sources of high cyanide consumption for a biooxidised refractory gold concentrate. In R. Amils, and A. Ballester, Process Metallurgy 9A, Biohydrometallurgy and the environment toward the mining of the 21st century (Vol. 9, pp. 337-346). Madrid, Spain: Elsevier.

Komnitsas, C. and Pooley, F. (1990). Bacterial oxidation of an arsenical gold sulfide concentrate from Olympias, Greece. Minerals Engineering, 3(3/4), 295-306.

Kondos, P., Deschenes, G. and Morrison, R. (1995). Process optimisation studies in gold cyanidation. Hydrometallurgy, 39, 235-250.

Kuyucak, N. (2001). Acid Mine Drainage (AMD) – treatment options for mining effluents. Mining Environment Management Journal, March 2001 Issue, pp. 14-17.

Kuyucak, N. and Akcil, A. (2013). Cyanide and removal options from effluents in gold mining and metallurgical processes. Minerals Engineering, 50-51, 13-29

La Brooy, S., Linge, H. and Walker, G. (1994). Review of gold extraction from ores. Minerals Engineering, 7(10), 1213-1241.

Levenspiel, O. (1999). Chemical Reaction Engineering, third edition, Wiley, 580

Lynn, N. (1997). The bioleaching and processing of refractory gold ore. Journal of Minerals, Metals and Materials, 49(4), 24-31.

Madden, M., Madden, A., Rimstidt, J., Zahrai, S., Kendall, M. and Miller, M. (2012). Jarosite dissolution rates and nanoscale mineralogy. Geochimica et Cosmochimica Acta, 91, 306-321.

Marsden, J. and House, C. (2009). The Chemistry of Gold Extraction (2nd ed.). Society for Mining, Metallurgy, and Exploration.

Martell, A. and Smith, R. (1989). Critical stability constants. Plenum.

Miller, P. and Brown, A. (2005). Bacterial oxidation of refractory gold concentrates. In Adams, M.D. (Ed.), Developments in Mineral Processing, 15, 371-401.

Nicol, M., and Scott, P. (1979). The kinetics and mechanism of the non-oxidative dissolution of some iron sulfides in aqueous acidic solutions. Journal of the South African Institute of Mining and Metallurgy, 79, 298-305.

Nicol, M., Fleming, C. and Paul, R. (1987). The chemistry of the extraction of gold. In Stanley, G. The Extractive Metallurgy of Gold in South Africa (Vol. 1).The South African Institute of Mining and Metallurgy.

Nicol, M., Senanayake, G. and Welham, N. (2006). Hydrometallurgy - Theory and Practice - Fundamentals (Vol. Module 9). Perth, Australia: Minerals Council of Australia.

Niemela, S., Riekkola-Vanhanen, M., Sivela, C., Viguera, F., and Tuovinen, O. (1994). Nutrient effect on the biological leaching of black-schist ore. Applied and environmental microbiology, 60 (4), 1297-1291.

Pachla, S., Taylor, R. and DeLorey, J. (1991, November 12). Patent No. 5063997. United States of America.

Patino, F., Cruells, M., Roca, A., Salinas, E. and Perez, M. (2003). Kinetics of alkaline decomposition and cyanidation of argentian ammonium jarosite in lime medium. Hydrometallurgy, 70, 153-161.

Patino, F., Reyes, I., Flores, M., Pandiyan, T., Roca, A., Reyes, M. (2013). Kinetic modelling and experimental design of the sodium arsenojarosite decomposition in alkaline media: Implications. Hydrometallurgy, 137, 115-125.

Patino, F., Salinas, E., Cruells, M. and Roca, A. (1998). Alkaline decomposition-cyanidation kinetics of argentian natrojarosite. Hydrometallurgy, 49, 323-336.

Pritchett, B., Madden, M. and Madden, A. (2012). Jarosite dissolution rates and maximum lifetimes in high salinity brines: Implications for Earth and Mars. Earth and Planetary Science Letters, 357-358, 327-336.

Roca, A., Cruells, M., Patino, F., Rivera, I. and Plata, M. (2006). Kinetic model for the cyanidation of silver ammonium jarosite in NaOH medium. Hydrometallurgy, 81, 15-23.

Roca, A., Patino, F. V. and Nunez, C. (1993). Alkaline decomposition-cyanidation kinetics of argentojarosite. Hydrometallurgy, 33, 341-358.

Salinas, E., Roca, A., Cruells, M., Patino, F., and Cordoba, D. (2001). Characterization and alkaline decomposition-cyanidation kinetics of industrial ammonium jarosite in NaOH media. Hydrometallurgy, 60, 237-246.

Sand, W., Gehrke, T., Jozsa, P. and Schippers, A. (2001). (Bio)chemistry of bacterial leaching – direct vs. indirect bioleaching. Hydrometallurgy, 59, 159–175.

Sand, W., Gehrke, T., Hallman, R. and Schippers, A. (1995). Sulfur chemistry, biofilm, and the (in)direct attack mechanism – a critical evaluation of bacterial leaching. Applied Microbiol Biotechnology, 43, 961–966.

Schippers, A. and Sand, W. (1999). Bacterial leaching of metal sulfides proceeds by two indirect mechanisms via thiosulfate or via polysulfides and sulfur. Applied and Environmental Microbiology, 66 (1), 319-321

Sehmel, G. (1989). Cyanide and antimony thermodynamic data base for the aqueous species and solids for the EPA-MINTEQ geochemical code. 33-35. (P. N. laboratory, Compiler) Richland, Washington.

Sharpe, A. (1976). The chemistry of cyano complexes of the transition metals. London: Academic press.

Stumm, W. and Morgan, J. (1996). Aquatic chemistry (Third ed.). New York: Wiley-Interscience.

Sun, L., Zhang, X., Tan, W. and Zhu, M. (2012). Effects of dissolved oxygen on the biooxidation process of refractory gold ores. Journal of Bioscience and Bioengineering, 114(5), 531–536.

Tanaka, M., Yamaji, Y., Fukano, Y., Shimanda, K., Ishibashi, J. and Hirajima, T. (2015). Biooxidation of gold-, silver, and antimony-bearing highly refractory polymetallic sulfide concentrates, and its comparison with abiotic pretreatment techniques. Geomicrobiology, 32, 538-548.

Van Aswegen, P., Godfrey, M., Miller, D. and Haines, A. (1989). Design and operation of a commercial bacterial oxidation plant at Fairview. Perth International Gold Conference, 89, 127-144.

Van Aswegen, P.C. and van Niekerk, J. (2004). New developments in the bacterial oxidation technology to enhance the efficiency of the BIOX® process. Proceedings of Bac-Min Conference. Carlton, Victoria, Australia: Australasian Institute of Mining and Metallurgy, 181-189.

Van Aswegen, P., Van Niekerk, J. and Olivier, W. (2007). The BIOX™ Process for the treatment of refractory gold concentrates. In Rawlings, D. and Johnson, D., Biomining (Chapter 1). Berlin Heidelberg: Springer-Verlag.

Vogel, A. (1979). Textbook of macro and semimicro qualitative inorganic analysis (Fifth ed.). (Sevhla, G. Ed.) London and New York: Longman.

Wang, X. and Forssberg, K. (1990). The chemistry of cyanide-metal complexes in relation to hydrometallurgical processes of precious metals. Mineral processing and extractive metallurgy review , 6, 81-125.

Wang, H., Bigham, J., Jones, S. and Tuovinen, O. (2007). Synthesis and properties of ammoniojarosites prepared with iron-oxidising acidophilic microorganisms at 22-65ºC. Geochemica et Cosmochimica Acta, 71, 155-164.

Welch, A., Kirste, D., Christy, A., Beavis, F. and Beavis, S. (2008). Jarosite dissolution II - Reaction kinetics, stoichiometry and acid flux. Chemical Geology, 254, 73-86.

7 APPENDICES

Appendix 1. Gibbs Free Energy Data, Database NBS 25°C for the sulfur (1M), potassium (1M) and iron (1M) system

Species	ΔG^o kJ/mole	Species	ΔGo kJ/mole
K^+ *A*	**-283.2694**	SO_3^{2-} *A*	-486.4988
KOH *O A*	-437.228	**SO_4^{2-} *A***	**-744.5303**
K O *S*	0	$S_2O_3^{2-}$ *A*	-522.5021
K_2O *O S*	-239.4001	$HS_2O_3^-$ *A*	-532.2048
K_2O_2 *O S*	-425.0986	$H_2S_2O_3$ *O A*	-535.552
KOH *O S*	-379.0788	$S_2O_3^{2-}$ *A*	600.2994
KOH:H_2O *O S*	-645.1017	$S_2O_8^{2-}$ *A*	1114.898
KOH:2H_2O *O S*	-887.3009	$S_4O_6^{2-}$ *A*	1040.402
Fe^{2+} *A*	**-78.90187**	HS^- *A*	12.07921
Fe^{3+} *A*	**-4.698632**	H_2S *O A*	-27.83197
$FeOH^+$ *A*	-277.3992	HSO_3^- *A*	-527.7321
$Fe(OH)_2$*O A*	**-447.0604**	HSO_4^- *A*	-755.9108
$Fe(OH)^{2+}$ *A*	-229.4087	H_2SO_3 *O A*	-537.8113
$Fe(OH)_2^+$ *A*	-438.002	$HS_2O_4^-$ A	-614.4999
$Fe(OH)_3$*O A*	**-659.3021**	$H_2S_2O_4$ *A*	-616.6003
$Fe(OH)_3^-$ *A*	-614.9016	HSO_5^- *A*	-637.5161
$Fe(OH)_4^{2-}$ *A*	-769.7012	$S_2O_5^{2-}$ *A*	-790.776
$Fe(OH)_2^{4+}$ *A*	-467.2691	$S_2O_6^{2-}$ *A*	-966.504
$Fe(OH)_4^-$ *A*	**-842.4484**	$S_3O_6^{2-}$ *A*	-958.136
$FeSO_4^+$ *A*	**-772.7011**	$S_5O_6^{2-}$ *A*	-958.136
$Fe(SO_4)_2^-$ *A*	-1524.499	S *O S*	0
Fe *O S*	0	S *O L*	0.389112
$Fe_{0.947}O$ *O S* Wustite	-245.1196	SO_3 *O S*	-374.2086
Fe_2O_3*O S* Hematite	-742.1998	SO_3 *O L*	-373.7484
Fe_3O_4*O S* Magnetite	-1015.398	H_2SO_4 O L	-690.0043
$Fe(OH)_2$ *O S* ppt	**-486.4988**	H_2SO_4:H_2O *O L*	-950.3831
$Fe(OH)_3$ *O S* ppt	**-696.4979**	H_2SO_4:2H_2O *O L*	-1199.649
FeS *O S* Pyrrhotite-Fe	**-100.3993**	H_2SO_4:3H_2O *O L*	-1443.982

FeS_2 *O S* Pyrite	**-166.8998**	$H_2SO_4{:}4H_2O$ *O L*	1685.863
Fe_7S_8 *O S* Pyrrhotite-S	-748.5009	$H_2SO_4{:}6.5H_2O$ *O L*	-2285.736
$FeSO_4$ *O S*	-820.8004	$KHSO_4$ *O A*	-1018.386
$FeSO_4{:}7H_2O$ *O S*	-2509.869	KSO_4^- *A*	-1032.072
$KFe_3(SO_4)_2(OH)_6$ *O S* Jarosite K	**-3293.11**	$KS_2O_8^-$ *A*	-1403.201
$H_2Fe_3(SO_4)_2(OH)_7$ *O S* Jarosite H	**3231.558**	K_2S *O S*	-363.9996
S^{2-} *A*	**85.80128**	K_2SO_4 *O S*	-1321.37
S_2^{2-} *A*	79.50018	$K_2S_2O_7$ *O S*	-1791.501
S_3^{2-} *A*	73.70116	$K_2S_2O_8$ *O S*	-1697.298
S_4^{2-} *A*	69.09875	$K_2S_4O_6$ *O S*	-1613.342
S_5^{2-} *A*	65.70135	$KHSO_4$ O S	-1031.302

NB

Items in bold considered in the diagram

A – aqueous, S – solid, L – liquid, O – neutral, ppt - precipitate

Appendix 2. Gibbs Free Energy Data, Database NBS 25°C for the cyanide (0.001M) and iron (0.006M) system

Species	ΔG^o kJ/mole	Species	ΔG^o kJ/mole
CN^- *A*	**172.4017**	$Fe(OH)_4^-$ *A*	-842.4484
HCN *O A*	**119.7001**	**Fe O *A***	**0**
HCN *O L*	124.9714	$Fe(OH)_2$ *O S* ppt	-486.4988
Fe^{2+} *A*	**-78.90187**	**$Fe(OH)_3$ *O S* ppt**	**-696.4979**
Fe^{3+} *A*	**-4.698632**	**$Fe(CN)_6^{3-}$ *A***	**729.4009**
$FeOH^+$ *A*	-277.3992	**$Fe(CN)_6^{4-}$ *A***	**695.0796**
$Fe(OH)_2$ *O A*	-447.0604	$HFe(CN)_6^{3-}$ *A*	671.2801
$FeOH^{2+}$ *A*	-229.4087	$H_2Fe(CN)_6^{2-}$ *A*	658.5992
$Fe(OH)_2^+$ *A*	-438.002	$Fe_{0.947}O$ *O S* Wustite	-245.1196
$Fe(OH)_3$ *O A*	**-659.3021**	Fe_2O_3 *O S* Hematite	-742.1998
$Fe(OH)_3^-$ *A*	**-614.9016**	Fe_3O_4 *O S* Magnetite	-1015.398
$Fe(OH)_4^{2-}$ *A*	-769.7012		
$Fe(OH)_2^{4+}$ *A*	-467.2691		

NB

Items in bold considered in the diagram

A – aqueous, S – solid, L – liquid, O – neutral, ppt - precipitate

Appendix 3. Jarosite precipitation and decomposition calculations

Jarosite precipitation calculations

Initial iron (+3) added in 1 litre is 46.0g $Fe_2(SO_4)_3$:9.5H_2O

$55.85x2/_{570.7}$ = 9.00 g Fe $9.00\ g/L/_{55.85\ g/mole}$ = 0.161M

Residual iron (+3) in solution 1.24 g/L $1.24g/L/_{55.85g/mole}$ = 0.022M

$1.24g/Lx100\%/_{9.00g/L}$ = 13.8% mass/mass

Precipitated iron (+3) = 9.00 – 1.24 = 7.76 g/L

$7.76g/Lx100\%/_{9.00g/L}$ = 86.2% mass/mass

Concentration of Fe^{3+} at pH 2.2 read from Figure 4.1.

Fe^{3+} log(mols/L) = -4.28 $[Fe^{3+}] = 5.2 \times 10^{-5}$M

Jarosite decomposition calculations

Average iron content in jarosite decomposition product 48.9 % mass/mass

Iron in $Fe(OH)_3$ $55.85x100\%/_{106.85}$ = 52.3% mass/mass

Appendix 4. Gibbs Free Energy Data, Database NBS 25°C for the solubility of iron in sulfur (0.316M) and potassium (0.28M)

Species	ΔG^o kJ/mole	Species	ΔG^o kJ/mole
SO_4^{2-} *A*	**-744.5303**	$Fe_3(OH)_4^{5+}$ *A*	-926.0824
HSO_4^- *A*	-755.9108	$Fe(OH)_3$ *O S* Ferrihydrite	-687.9764
SO_3 *O S*	-374.2086	$Fe_2(SO_4)_3$ *O S*	-2222.177
SO_3 *O L*	-373.7484	**$KFe_3(SO_4)_2(OH)_6$ *O S* Jarosite K**	**-3293.11**
H_2SO_4 O L	-690.0043	**$H_2Fe_3(SO_4)_2(OH)_7$ *O S* Jarosite H**	**3231.558**
$H_2SO_4:H_2O$ *O L*	-950.3831	**Fe^{3+} *A***	**-4.698632**
$H_2SO_4:2H_2O$ *O* L	-1199.646	$Fe(OH)^{2+}$ *A*	-229.4087
$H_2SO_4:3H_2O$ *O L*	-1443.982	$Fe(OH)_2^+$ *A*	-438.002
$H_2SO_4:4H_2O$ *O L*	-1685.863	**$Fe(OH)_3$ *A***	**-659.3021**
$H_2SO_4:6.5H_2O$ *O L*	-2285.736	$Fe_2(OH)_2^{4+}$ *A*	-467.2691
K^+ *A*	-283.2694	$Fe(OH)_4^-$ *A*	-842.4484
KOH *O A*	-437.228	**$FeSO_4^+$ *A***	**-772.7011**
$KHSO_4$ *O A*	-1018.386	**$Fe(SO_4)_2^-$ *A***	**-1524.499**
KSO_4^- *O A*	-1032.072	Fe_2O_3 *O S* Hematite	-742.1998
KOH *O S*	-379.0788	**$Fe(OH)_3$ *O S* ppt**	**-696.4979**
$KOH:H_2O$ *O S*	-645.1017	$HFeO_2$ *O S* Goethite	-475.9129
K_2SO_4 *O S*	-13121.37	FeOOH *O S* Lepidocrite	-470.941
$K_2S_2O_7$ *O S*	-1791.501	Fe_2O_3 *O S* Maghemite	-683.9531
$KHSO_4$ *O S*	-1031.302		

NB

Items in bold considered in the diagram

A – aqueous, S – solid, L – liquid, O – neutral, ppt - precipitate

Appendix 5. Particle size distribution calculations for the jarosite

Particle size (µm)	Log (particle size)	Volume (%)	Cumulative % volume retained	log (cumulative % volume retained)	log (log(cumulative % volume retained))
0.275	-0.5607	1.28	1.28	0.1072	-0.9698
0.316	-0.5003	0.88	2.16	0.3345	-0.4757
0.363	-0.4401	1.09	3.25	0.5119	-0.2908
0.417	-0.3799	1.28	4.53	0.6561	-0.1830
0.479	-0.3197	1.43	5.96	0.7752	-0.1106
0.550	-0.2596	1.54	7.50	0.8751	-0.0580
0.631	-0.2000	1.60	9.10	0.9590	-0.0182
0.724	-0.1403	1.63	10.73	1.0306	0.0131
0.832	-0.0799	1.61	12.34	1.0913	0.0380
0.955	-0.0200	1.57	13.91	1.1433	0.0582
1.096	0.0398	1.52	15.43	1.1884	0.0750
1.259	0.1000	1.47	16.90	1.2279	0.0892
1.445	0.1599	1.46	18.36	1.2639	0.1017
1.660	0.2201	1.49	19.85	1.2978	0.1132
1.905	0.2799	1.57	21.42	1.3308	0.1241
2.188	0.3400	1.72	23.14	1.3644	0.1349
2.512	0.4000	1.91	25.05	1.3988	0.1458
2.884	0.4600	2.13	27.18	1.4342	0.1566
3.311	0.5200	2.36	29.54	1.4704	0.1674
3.802	0.5800	2.57	32.11	1.5066	0.1780
4.365	0.6400	2.76	34.87	1.5425	0.1882
5.012	0.7000	2.90	37.77	1.5771	0.1979
5.754	0.7600	3.02	40.79	1.6106	0.2070
6.607	0.8200	3.10	43.89	1.6424	0.2155
7.586	0.8800	3.16	47.05	1.6726	0.2234
8.710	0.9400	3.21	50.26	1.7012	0.2308
10.000	1.0000	3.27	53.53	1.7286	0.2377
11.482	1.0600	3.32	56.85	1.7547	0.2442

13.183	1.1200	3.38	60.23	1.7798	0.2504
15.136	1.1800	3.44	63.67	1.8039	0.2562
17.378	1.2400	3.50	67.17	1.8272	0.2618
19.953	1.3000	3.55	70.72	1.8495	0.2671
22.909	1.3600	3.58	74.30	1.8710	0.2721
26.303	1.4200	3.57	77.87	1.8914	0.2768
30.200	1.4800	3.50	81.37	1.9105	0.2811
34.674	1.5400	3.36	84.73	1.9280	0.2851
39.811	1.6000	3.12	87.85	1.9437	0.2886
45.709	1.6600	2.80	90.65	1.9574	0.2917
52.481	1.7200	2.41	93.06	1.9688	0.2942
60.256	1.7800	1.98	95.04	1.9779	0.2962
69.183	1.8400	1.54	96.58	1.9849	0.2977
79.433	1.9000	1.14	97.72	1.9900	0.2988
91.201	1.9600	0.81	98.53	1.9936	0.2996
104.713	2.0200	0.55	99.08	1.9960	0.3002
120.226	2.0800	0.37	99.45	1.9976	0.3005
138.038	2.1400	0.26	99.71	1.9987	0.3008
158.489	2.2000	0.18	99.89	1.9995	0.3009
181.970	2.2600	0.11	100.00	2.0000	0.3010

Coefficient of variation (CV) for Rosin-Rammler-Bennet calculated using the log (particle size um) and log(log cumulative % volume retained) values is 0.15

Coefficient of variation (CV) for Gate-Gaudin-Schuhmann calculated using the log (particle size um) and log(cumulative % volume retained) values is 0.5

Appendix 6. Particle size distribution for the jarosite decomposition products (amorphous $Fe(OH)_3$)

Particle size (µm)	Volume (%)	Cumulative % volume retained
0.275	0.26	0.26
0.316	0.44	0.70
0.363	0.67	1.37
0.417	0.88	2.25
0.479	1.07	3.32
0.550	1.23	4.55
0.631	1.36	5.91
0.724	1.47	7.38
0.832	1.57	8.95
0.955	1.68	10.63
1.096	1.80	12.43
1.259	1.95	14.38
1.445	2.14	16.52
1.660	2.36	18.88
1.905	2.60	21.48
2.188	2.84	24.32
2.512	3.07	27.39
2.884	3.27	30.66
3.311	3.42	34.08
3.802	3.51	37.59
4.356	3.55	41.14
5.012	3.55	44.69
5.754	3.53	48.22
6.607	3.49	51.71
7.586	3.46	55.17
8.710	3.44	58.61
10.000	3.43	62.04
11.482	3.43	65.47
13.183	3.43	68.90

15.136	3.42	72.32
17.378	3.40	75.72
19.953	3.36	79.08
22.909	3.28	82.36
26.303	3.15	85.51
30.200	2.95	88.46
34.674	2.68	91.14
39.811	2.35	93.49
45.709	1.97	95.46
52.481	1.57	97.03
60.256	1.17	98.20
69.183	0.82	99.02
79.433	0.52	99.54
91.201	0.31	99.85
104.713	0.12	99.97
120.226	0.03	100.00

Appendix 7. Conversion of the jarosite in alkaline media at pH 11 and 25°C following the concentration of potassium in solution with calculated shrinking core fractional conversion functions for different rate controlling steps

Time (min)		**10**	**20**	**30**	**40**	**50**	**60**	**70**	**80**	**90**	**100**
Run 1 (X)		0.39	0.50	0.51	0.55	0.62	0.66	0.66	0.70	0.70	0.70
Run 2 (X)		0.37	0.48	0.51	0.58	0.64	0.68	0.68	0.72	0.71	0.73
Average (X)		0.38	0.49	0.51	0.57	0.63	0.67	0.67	0.71	0.71	0.72
X	Sphere; film diffusion rate controlling	0.38	0.49	0.51	0.57	0.63	0.67	0.67	0.71	0.71	0.72
$1-3(1-X)^{2/3} + 2(1-X)$	Sphere; ash diffusion controlling	0.06	0.11	0.12	0.15	0.19	0.23	0.23	0.27	0.27	0.28
$1- (1-X)^{1/3}$	Shrinking sphere; reaction controlling	0.15	0.20	0.21	0.25	0.28	0.31	0.31	0.34	0.34	0.35

X = Fractional conversion; Conversions as a function of time taken from Levenspiel (1999).

Appendix 8. Results for the mass percent iron leached from jarosite decomposition product in alkaline cyanide aqueous solution at pH 10.5 – 11, 25°C for 24 hours as a function of cyanide in solution

NaCN (g/L)	1	2	3	Average	Standard deviation
	mass percent	mass percent	mass percent	mass percent	
0	0	0	0	0	-
1	0.7	0.7	0.8	0.7	0.1
2	2.1	1.9	2.2	2.1	0.2
3	6.4	6.3	6.2	6.3	0.1
4	8.0	8.2	8.1	8.1	0.1
5	13.1	12.4	12.9	12.8	0.4
6	14.1	13.2	13.2	13.5	0.5
7	20.3	19.7	19.9	2.02	0.3
8	23.6	22.9	23.5	23.2	0.4
9	27.3	26.9	26.8	27.0	0.3
10	34.2	33.2	33.2	33.5	0.6

Appendix 9. Results for the mass percent of iron leached from jarosite in alkaline aqueous cyanide solution after alkaline preconditioning at pH 10.5 - 11 and 25°C for periods ranging from 0 to 24 hours before adding NaCN at 8g/l

Preconditioning time (hours)	Run 1	Run 2	Run 3	Average	Standard deviation
	mass percent	mass percent	mass percent	mass percent	
0	25.3	24.1	23.8	24.4	0.8
3	14.3	16.1	15.7	15.4	0.9
6	12.9	14.5	13.9	13.8	0.8
9	12.1	12.9	13.1	12.7	0.5
15	10.9	10.0	10.6	10.5	0.5
18	10.2	9.9	9.8	10.0	0.2
21	9.4	8.8	8.7	9.0	0.4
24	8.9	8.2	8.1	8.4	0.4

Appendix 10. Results for the dissolution of jarosite in aqueous organic acids after 6 hours at 25°C

Organic acid	1	2	3	Average	Standard deviation
	mass percent	mass percent	mass percent	mass percent	
Oxalic	100	100	100	100	-
Tartaric	32	28	27	29	3
Citric	12	9	8	10	2

Appendix 11. Sieve analysis results for the pilot plant mesophile biooxidation product as received from the mine

Sieve size (µm)	1	2	3	Average	Standard deviation	mass percent passing
	mass percent retained	mass percent retained	mass percent retained	mass percent retained		
212	-	-	-	-	-	100
150	1	0.8	1.0	0.9	0.1	99
75	1.8	1.9	1.6	1.8	0.2	97
53	2.3	2.0	2.4	2.2	0.2	95

Appendix 12. Sieve analysis results for the pilot plant thermophile sample as received from the mine

Sieve size (µm)	1	2	3	Average	Standard deviation	mass percent passing
	mass percent retained	mass percent retained	mass percent retained	mass percent retained		
212	-	-	-	-	-	100
150	-	-	-	-	-	100
75	0.6	0.7	0.7	0.7	0.1	99
53	1.2	1.2	1.3	1.2	0.1	98

Appendix 13. XRD pattern of the pilot plant mesophile biooxidation product

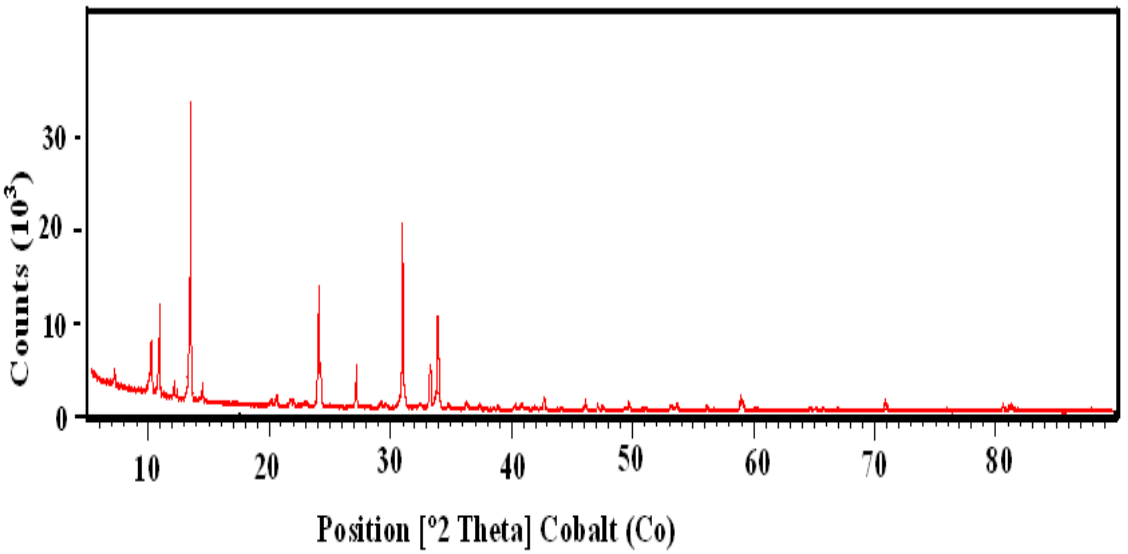

Appendix 14. XRD pattern of the pilot plant thermophile biooxidation product

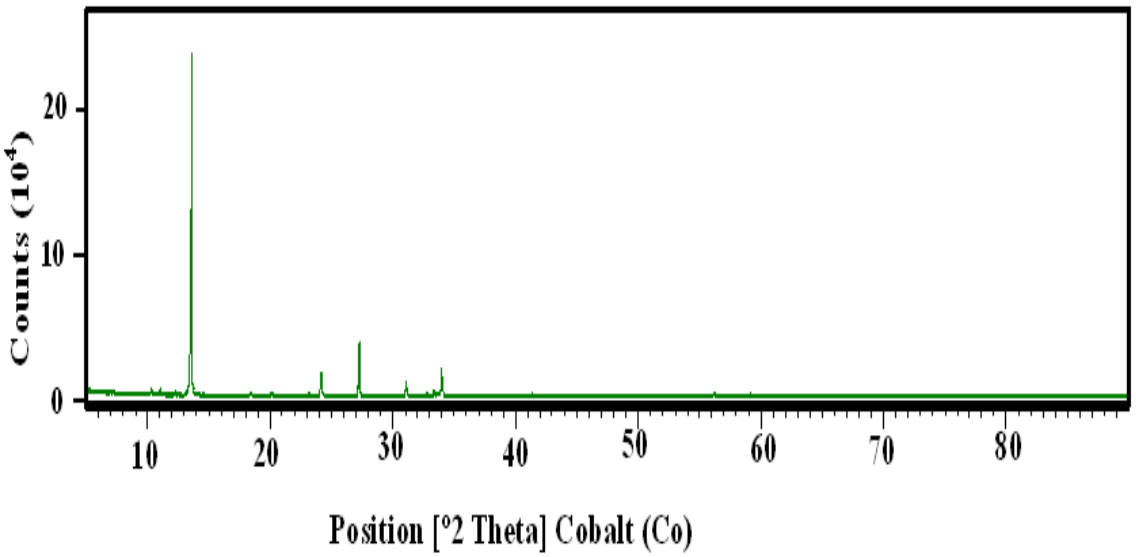

Appendix 15. XRD analytical results for the pilot plant mesophile biooxidation sample

Mineral	1	2	3	Average	Standard deviation
	mass percent	mass percent	mass percent	mass percent	
Jarosite	8	5	8	7	1
Gypsum	26.8	26.7	26.8	26.8	0.1
Chlorite	4	5	4	4	1
Hornblende	5	5	4	4	1
Muscovite	18	20	17	18	2
Quartz	29	31	29	30	1
Talc	10	7	12	10	2

Appendix 16. XRD analytical results for the pilot plant thermophile biooxidation sample

Mineral	1	2	3	Average	Standard deviation
	mass percent	mass percent	mass percent	mass percent	
Jarosite	14.3	15.1	15.0	14.8	0.4
Gypsum	46	48	46	47	1
Scorodite	10.2	11.6	10.0	10.6	0.9
Chlorite	1.7	1.8	1.5	1.7	0.2
Hornblende	2.1	1.0	1.1	1.4	0.6
Muscovite	8	3	8	6	3
Quartz	14.6	16.1	15	15.2	0.7
Talc	3.1	3.7	3.6	3.5	0.3

Appendix 17. XRD analytical results for the pilot plant mesophile cyanide leach residue

Mineral	1	2	3	Average	Standard deviation
	mass percent	mass percent	mass percent	mass percent	
Jarosite	5.8	6.0	5.6	5.8	0.2
Gypsum	23	25	23	23	1
Chlorite	2.6	3.6	3.2	3.1	0.5
Hornblende	4.6	3.2	3.8	3.8	0.7
Muscovite	19.6	20.6	21.0	20.4	0.7
Quartz	32.9	32.4	31.5	32.3	0.7
Talc	9.9	9.2	10.9	10.0	0.8
Scorodite	1.4	0.5	1.4	1.1	0.5

Appendix 18. XRD analytical results for the pilot plant thermophile cyanide leach residue

Mineral	1	2	3	Average	Standard deviation
	mass percent	mass percent	mass percent	mass percent	
Jarosite	12.5	12.5	13.0	12.7	0.3
Gypsum	47.4	47.0	47.4	47.3	0.2
Scorodite	10.4	10.4	9.8	10.2	0.3
Chlorite	1.1	1.2	1.4	1.2	0.2
Hornblende	2.07	2.04	2.03	2.05	0.02
Muscovite	8.0	7.9	7.9	7.9	0.1
Quartz	15.4	16.0	15.8	15.7	0.3
Talc	3.1	2.6	2.7	2.8	0.2

Appendix 19. XRF analytical results of the pilot plant mesophile biooxidation product

Analyte	Sample 1	Sample 2	Sample 3	Average	Standard deviation
	mass percent	mass percent	mass percent	mass percent	
Si	23.0	22.4	22.4	22.6	0.4
S	5.9	6.2	6.2	6.1	0.2
Al	6.0	5.8	5.9	5.9	0.1
Ca	6.4	6.7	6.8	6.6	0.2
Fe	3.9	4.2	4.2	4.1	0.2
Mg	2.86	2.81	2.80	2.82	0.03
K	2.66	2.70	2.72	2.70	0.03
Ti	0.40	0.41	0.41	0.41	0.01
As	0.30	0.31	0.32	0.31	0.01
Na	0.24	0.20	0.19	0.21	0.02
Cr	0.16	0.18	0.18	0.18	0.01
P	0.03	0.04	0.04	0.04	0.01
Ni	0.047	0.054	0.053	0.052	0.004
Sb	0.042	0.045	0.046	0.044	0.002
Mn	0.035	0.038	0.037	0.037	0.001
Cu	0.0348	0.0341	0.0352	0.0347	0.0005
Ba	0.0344	0.0337	0.0331	0.0337	0.0006
V	0.0147	0.0151	0.0144	0.0147	0.0003
Pb	0.0218	0.0223	0.0236	0.0226	0.0009
Zr	0.0115	0.0121	0.0119	0.0118	0.0003
Au	0.0121	0.0122	0.0132	0.0125	0.0006
Rb	0.0097	0.0099	0.0105	0.0100	0.0004
Zn	0.0081	0.0091	0.0089	0.0087	0.0005
Co	0.0070	0.0076	0.0075	0.0074	0.0003
Sr	0.0066	0.0068	0.0071	0.0068	0.0003

Appendix 20. XRF analytical results of pilot plant mesophile biooxidation product cyanide leach residue

Analyte	Sample 1	Sample 2	Sample 3	Average	Standard deviation
	mass percent	mass percent	mass percent	mass percent	
Si	22.6	24.7	25.0	24.8	0.2
S	4.65	4.66	4.72	4.68	0.04
Al	6.3	6.2	6.0	6.1	0.1
Ca	6.7	6.7	6.9	6.8	0.1
Fe	3.5	3.5	3.1	3.4	0.2
Mg	2.47	2.45	2.51	2.48	0.03
K	3.0	2.9	2.8	2.9	0.1
Ti	0.399	0.401	0.391	0.397	0.005
As	0.25	0.25	0.20	0.23	0.03
Na	0.25	0.24	0.22	0.24	0.01
Cr	0.161	0.158	0.153	0.157	0.004
P	0.024	0.022	0.018	0.021	0.003
Ni	0.0158	0.0156	0.0157	0.0157	0.0001
Sb	0.040	0.041	0.038	0.040	0.002
Mn	0.0264	0.0267	0.0260	0.0264	0.0003
Cu	0.027	0.027	0.026	0.027	0.001
Ba	0.035	0.039	0.032	0.035	0.003
V	0.014	0.014	0.015	0.014	0.001
Pb	0.023	0.024	0.018	0.021	0.003
Zr	0.0119	0.0124	0.0117	0.0120	0.0003
Au	<0.01	<0.01	<0.01	<0.01	
Rb	<0.01	<0.01	<0.01	<0.01	
Zn	<0.01	<0.01	<0.01	<0.01	
Co	<0.01	<0.01	<0.01	<0.01	
Sr	<0.01	<0.01	<0.01	<0.01	

Appendix 21. XRF analytical results of the pilot plant thermophile biooxidation product

Analyte	Sample 1	Sample 2	Sample 3	Average	Standard deviation
	mass percent	mass percent	mass percent	mass percent	
Si	13.8	12.9	12.8	13.2	0.5
S	9.2	9.1	9.2	9.2	0.1
Al	3.4	3.2	3.2	3.3	0.1
Ca	11	13	13	12	1
Fe	11.9	10.3	10.5	10.9	0.9
Mg	0.93	0.97	0.93	0.94	0.02
K	2.0	1.8	1.8	1.8	0.1
Ti	0.30	0.26	0.26	0.27	0.02
As	4.6	4.3	4.3	4.4	0.2
Na	0.22	0.21	0.21	0.21	0.01
Cr	0.07	0.06	0.06	0.06	0.01
P	0.210	0.204	0.204	0.206	0.004
Ni	0.006	0.008	0.005	0.006	0.002
Sb	0.048	0.044	0.044	0.045	0.002
Mn	0.008	0.008	0.009	0.008	0.001
Cu	0.012	0.011	0.010	0.011	0.001
Ba	0.0115	0.0116	0.0120	0.0117	0.0002
V	0.0048	0.0045	0.0044	0.0046	0.0002
Pb	0.014	0.014	0.013	0.014	0.001
Zr	0.0068	0.0066	0.0044	0.0046	0.0002
Au	<0.01	<0.01	<0.01	<0.01	
Rb	0.0055	0.0054	0.0056	0.0055	0.0001
Zn	0.0048	0.0046	0.0049	0.0048	0.0002
Co	0.007	0.008	0.004	0.006	0.002
Sr	0.0099	0.0102	0.0107	0.0103	0.0004

Appendix 22. XRF analytical results of the pilot plant thermophile biooxidation product cyanide leach residue

Analyte	Sample 1	Sample 2	Sample 3	Average	Standard deviation
	mass percent	mass percent	mass percent	mass percent	
Si	12.5	13.1	13.3	13.0	0.4
S	8.2	9.1	8.7	8.7	0.5
Al	3.1	3.0	3.2	3.1	0.1
Ca	12.9	13.8	12.6	13.1	0.6
Fe	10.5	8.8	10.3	9.9	0.9
Mg	0.88	0.82	0.93	0.88	0.06
K	1.8	1.6	1.8	1.7	0.1
Ti	0.252	0.251	0.259	0.254	0.005
As	4.4	4.1	4.3	4.3	0.1
Na	0.43	0.35	0.53	0.44	0.09
Cr	0.058	0.057	0.060	0.058	0.002
P	0.21	0.18	0.21	0.20	0.02
Ni	<0.01	<0.01	<0.01	<0.01	
Sb	0.0398	0.0396	0.0405	0.0400	0.0005
Mn	0.0067	0.0074	0.0069	0.0070	0.0004
Cu	0.0083	0.0082	0.0078	0.0081	0.0003
Ba	<0.01	<0.01	<0.01	<0.01	
V	0.0045	0.0046	0.0055	0.0049	0.0005
Pb	0.013	0.010	0.014	0.012	0.002
Zr	0.0070	0.0074	0.0068	0.0071	0.0003
Au	<0.01	<0.01	<0.01	<0.01	
Rb	<0.01	<0.01	<0.01	<0.01	
Zn	<0.01	<0.01	<0.01	<0.01	
Co	<0.01	<0.01	<0.01	<0.01	
Sr	0.0107	0.0099	0.0107	0.0104	0.0005

Appendix 23. Cyanide distribution in leach solution at the end of the BIOX® pilot plant mesophile and thermophile samples leach tests

	Mesophile	Thermophile
Fe, mg/L	173	291
Fe, moles/L (10^{-3})	3.1	5.2
Assume 1 mole of Fe reacts with 6 moles of CN^- to form $Fe(CN)_6^{3-}$, therefore CN^- moles/L (10^{-3})	18.6	31.3
Mass of NaCN consumed by Fe(g)	0.91	1.53
Mass of NaCN added/L (g)	8	8
Mass percent NaCN consumed by Fe	11	19
Mass percent NaCN consumed by other metal ions	1.4	0.5
Mass percent free CN^-, SCN^-, etc.	87.6	80.5

Appendix 24. Contribution of metal ions to cyanide consumption for the pilot plant mesophile BIOX® product sample leach tests

Metal	**Concentration (mg/L)**	**Cyanide complex**	**Equivalent cyanide moles ($x10^{-4}$)**	**Mass of NaCN consumed (g)**
Cu	8	$Cu(CN)_3^{2-}$	3.88	0.019
Zn	3	$Zn(CN)_4^{2-}$	0.92	0.004
Ni	19	$Ni(CN)_4^{2-}$	12.94	0.063
Au	52	$Au(CN)_2^-$	5.28	0.027
Ag	2	$Ag(CN)_2^-$	0.37	0.002
			Total mass	0.114

Mass percent consumed by metal cyanide complexes (0.114g/8g) x 100 = 1.4%

Appendix 25. Contribution of metal ions to cyanide consumption for the pilot plant thermophile BIOX® product sample leach tests

Metal	Concentration (mg/L)	Cyanide complex	Equivalent cyanide moles ($x10^{-4}$)	Mass of NaCN consumed (g)
Cu	5	$Cu(CN)_3^{2-}$	2.36	0.012
Zn	1	$Zn(CN)_4^{2-}$	0.31	0.001
Ni	6	$Ni(CN)_4^{2-}$	4.09	0.020
Au	11	$Au(CN)_2^-$	1.12	0.005
Ag	0.3	$Ag(CN)_2^-$	0.06	-
			Total mass	0.039

Mass percent consumed by metal cyanide complexes (0.039g/8g) x 100 = 0.5%

Appendix 26. Results for the comparison of jarosite converted and dissolved during a 24 hour leach of synthetic and pilot plant process jarosites with 9 g/L NaCN added

	Jarosite converted to $Fe(OH)_3$					**Jarosite converted to $Fe(CN)_6^{3-}$**				
	1	2	3	Average	Standard deviation	1	2	3	Average	Standard deviation
	mass percent	mass percent	mass percent	mass percent		mass percent	mass percent	mass percent	mass percent	
Synthetic jarosite	100	100	100	100	-	51	49	47	49	2
Mesophile process	15	19	18	17	2	9	7	8	8	1
Thermophile process	13	12	16	14	2	7	5	7	6	1

Appendix 27. XRD analytical results of the main plant mesophile BIOX® product sample

Mineral	1	2	3	Average	Standard deviation
	mass percent	mass percent	mass percent	mass percent	
Chlorite	2.6	3.6	3.2	3.1	0.5
Gypsum	23	25	23	23	1
Hornblende	4.6	3.2	3.8	3.8	0.7
Jarosite	5.8	6.0	5.9	5.9	0.1
Muscovite	24.6	25.6	25.0	25.0	0.5
Quartz	32.9	32.4	31.5	32.3	0.7
Scorodite	1.42	1.38	1.40	1.40	0.02
Talc	4.9	4.2	4.6	4.6	0.3

Appendix 28. XRD analytical results of the main plant thermophile BIOX® product sample

Mineral	1	2	3	Average	Standard deviation
	mass percent	mass percent	mass percent	mass percent	
Chlorite	1.1	1.2	1.4	1.2	0.2
Goethite	0.41	0.39	0.48	0.43	0.05
Gypsum	45	46	47	46	1
Hornblende	1.8	2.0	2.0	1.9	0.2
Jarosite	16	15	13	14	2
Muscovite	8.0	7.7	7.9	7.9	0.2
Quartz	15.2	15.3	15.8	15.4	0.3
Scorodite	10.4	10.1	9.8	10.1	0.3
Talc	3.1	2.6	2.7	2.8	0.2

Appendix 29. XRF Analytical results of the main plant mesophile BIOX® product sample

Analyte	Sample 1	Sample 2	Sample 3	Average	Standard deviation
	mass percent	mass percent	mass percent	mass percent	
Si	25.3	25.4	25.2	25.3	0.1
S	3.5	3.2	3.5	3.4	0.1
Al	7.58	7.40	7.54	7.51	0.09
Ca	2.69	2.61	2.57	2.62	0.07
Fe	4.72	4.81	4.64	7.72	0.08
Mg	3.09	2.99	3.14	3.07	0.08
K	3.5	3.6	3.4	3.5	0.1
Ti	0.52	0.52	0.50	0.51	0.01
As	0.64	0.66	0.63	0.64	0.02
Na	0.22	0.19	0.20	0.20	0.01
Cr	0.17	0.16	0.18	0.17	0.01
P	0.06	0.05	0.06	0.06	0.01
Ni	0.071	0.063	0.055	0.063	0.008
Sb	0.033	0.025	0.033	0.031	0.005
Mn	0.031	0.039	0.031	0.034	0.004
Cu	0.064	0.064	0.056	0.061	0.005
Ba	0.027	0.045	0.036	0.036	0.009
V	0.017	0.011	0.022	0.017	0.006
Pb	0.06	0.06	0.07	0.06	0.01
Zr	0.015	0.015	0.022	0.017	0.004
Au	0.012	0.012	0.013	0.013	0.001
Rb	0.009	0.009	0.009	0.009	-
Zn	0.016	0.016	0.008	0.013	0.005
Co	0.007	0.007	0.007	0.007	-
Sr	0.007	0.008	0.008	0.008	0.001

Appendix 30. XRF Analytical results of the main plant thermophile BIOX® product sample

Analyte	Sample 1	Sample 2	Sample 3	Average	Standard deviation
	mass percent	mass percent	mass percent	mass percent	
Si	24.9	25.3	24.8	25.0	0.2
S	2.85	2.82	2.90	2.86	0.04
Al	6.23	6.11	6.30	6.21	0.09
Ca	1.01	1.03	0.99	1.01	0.02
Fe	8.9	8.6	8.9	8.8	0.2
Mg	3.3	3.1	3.3	3.3	0.1
K	3.0	2.6	2.9	2.8	0.2
Ti	0.40	0.35	0.37	0.38	0.02
As	2.0	2.1	1.8	2.0	0.2
Na	0.28	0.26	0.29	0.28	0.02
Cr	0.18	0.18	0.17	0.18	0.01
P	0.08	0.06	0.08	0.07	0.01
Ni	0.047	0.039	0.055	0.047	0.008
Sb	0.04	0.03	0.06	0.04	0.01
Mn	0.023	0.031	0.023	0.026	0.004
Cu	0.04	0.06	0.03	0.04	0.01
Ba	0.03	0.03	0.04	0.03	0.01
V	0.017	0.022	0.028	0.022	0.006
Pb	0.08	0.06	0.08	0.08	0.01
Zr	0.015	0.015	0.015	0.015	-
Au	0.012	0.012	0.013	0.013	0.001
Rb	0.009	0.009	0.009	0.009	-
Zn	0.008	0.008	0.008	0.008	-
Co	0.007	0.007	0.007	0.007	-
Sr	0.007	0.008	0.008	0.0008	0.001

Appendix 31. Results for iron leaching after 24 hours from main plant cyanidation feed mesophile and thermophile BIOX® products samples as a function of cyanide added at pH 10.5 and 25°C

	Mesophile					Thermophile				
NaCN kg/t ore	1 (mg/L)	2 (mg/L)	3 (mg/L)	Average (mg/L)	Standard deviation	1 (mg/L)	2 (mg/L)	3 (mg/L)	Average (mg/L)	Standard deviation
2	10	13	14	12	2	19	12	16	16	4
5	125	105	115	115	10	34	46	41	40	6
10	336	359	341	346	12	133	118	129	127	8
15	435	405	426	422	15	325	318	338	327	10
20	501	465	477	481	18	574	566	598	579	17

Appendix 32. Results for total sulfur leaching after 24 hours from main plant cyanidation feed mesophile and thermophile BIOX® products samples as a function of cyanide added at pH 10.5 and 25°C

	Mesophile					Thermophile				
NaCN kg/t ore	1 (mg/L)	2 (mg/L)	3 (mg/L)	Average (mg/L)	Standard deviation	1 (mg/L)	2 (mg/L)	3 (mg/L)	Average (mg/L)	Standard deviation
2	988	1123	950	1020	91	845	766	790	800	41
5	1380	1195	1295	1290	93	1190	1301	1230	1240	56
10	2765	2915	2855	2845	75	1638	1680	1715	1678	39
15	4105	3930	4010	4015	88	1895	1975	1905	1925	44
20	4170	4245	4150	4188	50	2305	2201	2245	2250	52

Appendix 33. Results for gold leaching after 24 hours from main plant cyanidation feed mesophile and thermophile BIOX® products samples as a function of cyanide added at pH 10.5 and 25°C

	Mesophile					Thermophile				
NaCN kg/t ore	1 (mg/L)	2 (mg/L)	3 (mg/L)	Average (mg/L)	Standard deviation	1 (mg/L)	2 (mg/L)	3 (mg/L)	Average (mg/L)	Standard deviation
2	29	27	27	28	1	41	41	43	42	1
5	30	33	31	31	2	52	55	54	54	2
10	42	39	39	40	2	56	55	56	56	1
15	53	50	49	51	2	54	52	53	53	1
20	64	70	69	68	3	54	56	55	55	1

Appendix 34. Results for free NaCN in solution after leaching for 24 hours from main plant cyanidation feed mesophile and thermophile BIOX® products samples as a function of cyanide added at pH 10.5 and 25°C

	Mesophile					Thermophile				
NaCN kg/t ore	1 (mg/L)	2 (mg/L)	3 (mg/L)	Average (mg/L)	Standard deviation	1 (mg/L)	2 (mg/L)	3 (mg/L)	Average (mg/L)	Standard deviation
2	-	-	-	-	-	1.1	1.1	1.3	1.2	0.1
5	-	-	-	-	-	6.4	5.8	5.9	6.0	0.3
10	-	-	-	-	-	10.1	10.6	10.7	10.5	0.3
15	-	-	-	-	-	13.1	13.8	13.6	13.5	0.4
20	-	-	-	-	-	16.9	17.2	17.7	17.3	0.4